IDEA League

Master of Science in Applied Geophysics

Research Thesis

Plate tectonics of New Zealand: insights from 3D thermomechanical modelling

Kittiphon Boonma

August 12, 2016

Plate tectonics of New Zealand: insights from 3D thermomechanical modelling

Master of Science Thesis

for the degree of Master of Science in Applied Geophysics at
Delft University of Technology
ETH Zürich
RWTH Aachen University
by

Kittiphon Boonma

August 12, 2016

Department of Geoscience & Engineering · Delft University of Technology
Department of Earth Sciences · ETH Zürich
Faculty of Georesources and Material Engineering · RWTH Aachen University

Delft University of Technology

Printed in The Netherlands, Switzerland, Germany

IDEA LEAGUE
JOINT MASTER'S IN APPLIED GEOPHYSICS

Delft University of Technology, The Netherlands
ETH Zürich, Switzerland
RWTH Aachen, Germany

Dated: *August 12, 2016*

Supervisor(s):

Prof. Dr. Taras Gerya (ETH Zurich)

Dr. Jie Liao (ETH Zurich)

Committee Members:

Prof. Dr. Taras Gerya (ETH Zurich)

Dr. Ranajit Ghose (TU Delft)

Abstract

New Zealand sits on an oblique convergent plate boundary between the Australian plate in the east, and the Pacific plate in the west. The tectonic setting comprises two opposing subduction zones, Hikurangi (ca. 25 Ma) in the north and Puysegur (ca. 20-6 Ma) in the south, and a transpressional continental transform fault, the Alpine Fault (ca. 23-22 Ma), linking the two subduction zones. Despite New Zealand being well-studied through several geological and geophysical methods, the dynamic evolution of the processes involved in the subduction zones and the continental transform are still not clear. An exploratory investigation, which employs 3D thermomechanical numerical modelling, is conducted in order to gain insights into the dynamic tectonic evolution of New Zealand. The finite-differences code ('I3ELVIS') iteratively solves the conservation laws (mass, momentum, and energy) in a staggered grid. The study focuses on three aspects of the dynamic evolution: (i) the 3D geometric and structural development; (ii) the topographic development; and (iii) the faults/stress development. Four sets of models are constructed to study the influence of prescribed weak-zones' geometry on New Zealand's tectonic evolution. The modelling results indicate that the continental transform system does not appear to be attaining a steady state. The results exhibit key tectonic features such as an oblique continental transform and the migration of subduction zones into the transform, all of which are consistent with natural observations. The interpretations of modelling results reflect (3D) structural development of the transform which are comparable to the interpretation of seismic survey transects. The observed key structural features are the steeply-dipping Alpine Fault, the thickening of the lower continental crust, and the presence of thrusting fault-blocks in the upper continental crust. An observed set of splay faults in the modelling results reflect the similarities, in faults and stress development, to the the Marlborough Fault System.

Acknowledgements

First of all, I would like to express my sincere gratitude to my supervisor, Prof. Taras Gerya, for giving me the opportunity to work on this project. His continuous supports and guidance were indispensable throughout this research project.

My sincerest thanks also go to Dr. Jie Liao for all of the insightful discussions we had. I am greatly appreciative of his advices and guidance, from software-related issues to professional development. His patience, motivation, and immense knowledge were vital to the completion of this project

Again, I thank both of my supervisors, not only for their insightful comments and encouragement, but also for the hard questions which incented me to widen my research from various perspectives. I could not have imagined having a better advisor and mentor for my Master thesis.

Lastly, I would like to thank my uncle, Anusorn, who has been financially supporting my education since a young age. I also thank Woranan for her moral support and understanding throughout these past 6 months. I could not have done this without her.

Swiss Federal Institute of Technology
August 12, 2016

Kittiphon Boonma

Table of Contents

List of Figures

List of Tables

Chapter 1

Introduction

New Zealand lies in the south-west Pacific Ocean. The micro-continent of New Zealand is composed of two tectonic settings: one **transpressional continental transform fault** (Alpine Fault) linking two **subduction zones** (Hikurangi and Puysegur). The zone of active tectonic plate collision takes place in the Alpine Fault which is located in the South Island.

The **Hikurangi Subduction Zone**, located on the eastern side of the North Island, is where the Pacific Plate subducts under the Australian Plate. Hikurangi margin was initiated ca. 25 Ma (King, 2000; Furlong, 2007), making it the first tectonic activity to initiate in this system. This westward oblique subduction zone is between the Oceanic Pacific Plate and the Continental Australian Plate. The Taupo Volcanic Zone in the North Island was formed as a result of this subduction.

The **Puysegur Subduction Zone** is located in the south of the South Island. It was initiated at around ca. 20-6 Ma (Lebrun et al., 2003), and formed by the subduction of the Australian Plate under the Pacific Plate. In contrast to the Hikurangi Subduction Zone, this eastward oblique subduction zone is between the oceanic Australian plate and the continental Pacific plate. The Puysegur margin was initiated after the Alpine Fault, making it the youngest tectonic development in the New Zealand system.

The **Alpine Fault**, a continental transform (hereinafter referred to as 'transforms') , formed in-between the two aforementioned subduction zones. Its evolution was largely controlled by the continent-continent collision, which gave rise to the mountain-building process that built the Southern Alps. The transform fault accommodates and transfers any displacement and plate motion between the Hikurangi and the Puysegur margins. The Alpine Fault developed a few million years after the initiation of the Hikurangi subduction zone. Transform faults are associated with 3D fault geometries which controls the segmentation, and thus, the size and timing of the associated earthquake. Even though several transform faults have been extensively studied, the evolution still remain an enigma, for example, the controlling processes, the coupling between the horizontal and vertical motions, the long-term kinetics, and the spreading out of the fault systems in the vicinity of the transforms.

The study of continental transform using numerical modelling exists since the 1980's. Over the last decade, there have been more and more generalised models of continental transform

boundary, expanding, both, in the scope of the numerical methods as well as the geological setting. So far, there have been 2 main modelling principles in the studying of continental transforms: (i) Generalised Numerical Models, which aim to study the general nature and tectonic behaviour of different transforms' characteristics e.g. the tectonic styles to be expected at obliquely converging plate boundaries (Braun and Beaumont, 1995), the interseismic behaviour of a strike-slip fault (Le Pourhiet et al., 2014), etc.; (ii) Models of Individual Continental Transforms e.g. for San Andreas Fault Systems and Dead Sea Transform. However, there has been no previous numerical modelling work done specifically on the Alpine Fault, or the whole of New Zealand for that matter; this project aims to initiate an exploratory investigation.

The tectonic settings, specifically the Alpine Fault, of New Zealand is one of the most complex systems. Despite New Zealand being well-studied through other geological and geophysical methods, the dynamic evolution of the processes involved in the subduction zones and the continental transform are still not clear. In an attempt to better understand the dynamic evolution of this micro-continent, 3D thermomechanical numerical modelling is employed to simulate the tectonic plate collisions that could have taken place.

The scope of this study focuses on three unconstrained aspects of tectonic evolution of New Zealand, namely:

1. the overall 3D geometry;
2. the development of topographic features; and
3. the development of faults.

The next introductory chapter will describe the geological and tectonic frameworks (Chapter 2), including the geology and tectonic setting of New Zealand, and specifically on continental transforms. The numerical method will be described in Chapter 3, including the underlying physical principles, as well as model setups. The results from the simulations will be described in the Chapter 4, which will then be followed by an overall discussion (Chapter 5) of the project and conclusion (Chapter 6).

Chapter 2

Geological Setting

This chapter aims to describe the geological and tectonic settings of New Zealand and, more specifically, of continental transforms. The chapter begins with the descriptions of the tectonics of New Zealand, including the tectonic evolution of New Zealand (Section 2-1-1), and geological setting of the Alpine Fault (Section 2-1-2). More details of the mechanical processes of transform faults are given in Section 2-2-1, and more specifically on the continental transform in Section 2-2-2.

2-1 Tectonic setting of New Zealand

The islands of New Zealand lie right above the plate boundary created by a continental-continental collision between the Pacific and Indo/Australian plates. The Alpine Fault is a continental transform fault which sits in-between the two subduction zones, Hikurangi margin (north) and Puysegur margin(south), whose dips are in an opposite direction. Topographic and bathymetric maps of New Zealand, and specifically of the South Island, are shown in Figure 2-1. In this section, the main geological and tectonic framework of New Zealand will be described.

The New Zealand micro-continent is composed of 3 parts: (i) Hikurangi (northern) and (ii) Puysegur (southern) subduction zones which are joined together by (iii) the transpressional Alpine Fault. The evolution history of these 3 components are of importance to the understanding of the underlying tectonic frameworks of the current geometry as well as the plate boundary kinematics.

2-1-1 Subduction Zones of New Zealand

The subduction along the **Hikurangi** margin began ca. 25 Ma along a west-east structure in the northern side of the North Island (King, 2000; Furlong, 2007). In Hikurangi subduction zone, the Pacific plate (≈120 Ma in this region) subducts under the younger Australian plate.

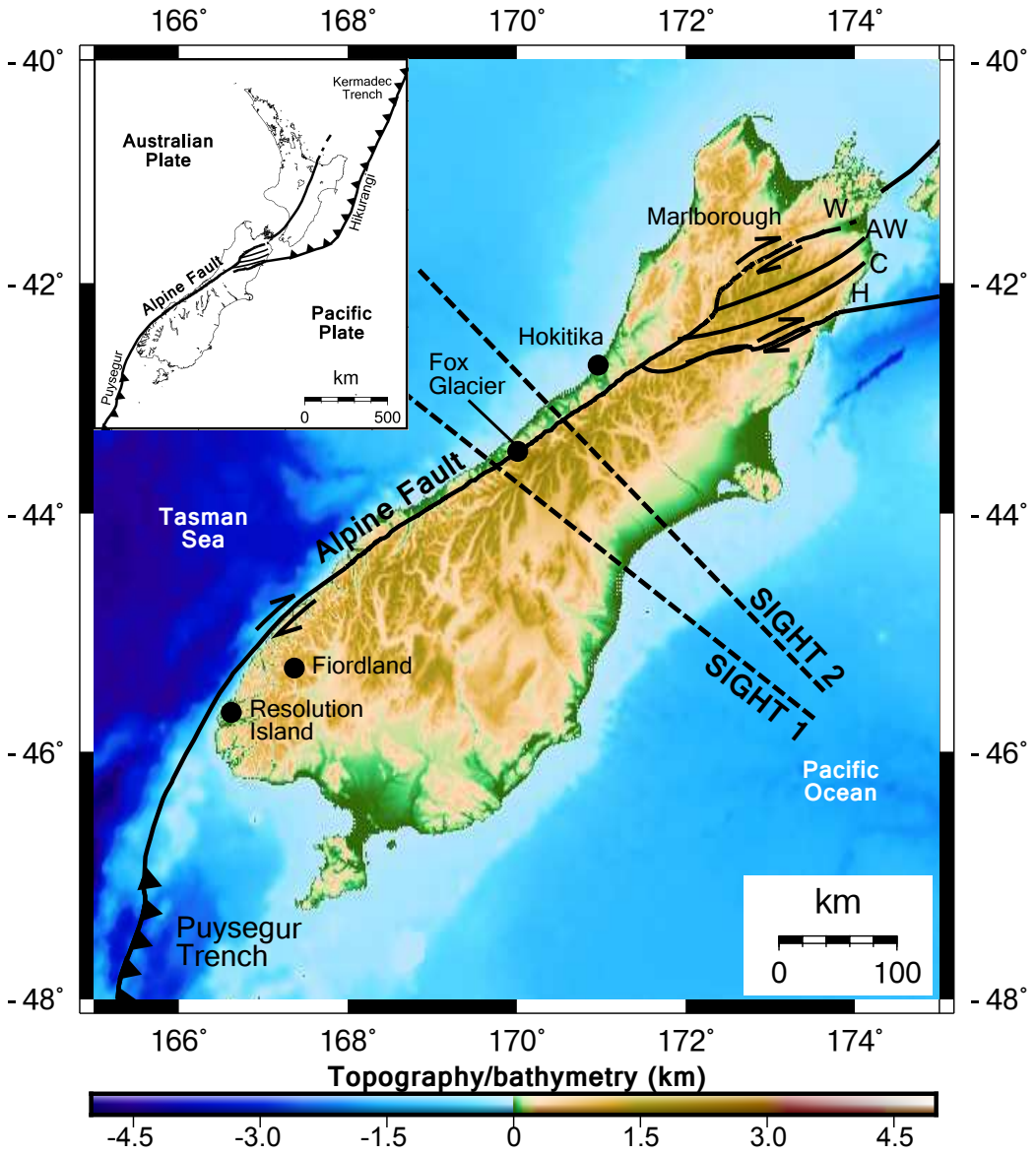

Figure 2-1: Topography/bathymetry map of the South Island. The Marlborough Fault System (Wairau Fault (W), Awatere Fault (AW), Clarence Fault (C), and Hope Fault (H)) is also shown. The dash lines indicate the SIGHT geophysical transects (Stern et al., 2007). The inset map shows the tectonic setting of New Zealand.

The zone is situated off the eastern side of the North Island (Figure 2-1). Towards the north, the Hikurangi zone continues into Kermadec Trench while continues and transitions into the transform fault (Alpine Fault) in the SSW direction. As a result from the relation plate motion between the Australian and the Pacific Plates, the southern segment of Hikurangi subducting slab migrated in the SSW direction. This obliquely convergent system caused north-west dipping Wadati-Banioff Zone to develop. The subduction zone exhibits complex nature in tectonic setting because the physical properties such as the convergent rate, the seismic coupling of the plate interface, and the surface heat flow change significantly along the strike (Yabe et al., 2014).

The **Puysegur** subduction zone is located in the south-west of the South Island (Figure 2-1), and is where the Australian plate is subducting under the Pacific plate. The subduction at Puysegur Margin was initiated ca. 20-6 Ma (Lebrun et al., 2003). The subduction front is located along the 5500 m deep Puysegur Trench between the Resolution Ridge and 48°S (Lebrun et al., 2003). The Puysegur Trench can reach up to 6250 m deep in the south of 48°S. The evolution of Puysegur subduction zone is southward along the Puysegur Trench, with the mature structure in the north of 48°S and an early stage in he south of 49°S. The transition of which the Puysegur subducting lithosphere makes, northward, into the Alpine Fault system still carries some uncertainties. A few plausible scenarios had been proposed: (i) a tear fault had developed within the western edge of the subducted Australian plate, allowing the Alpine Fault to form as a transform plate boundary (Lebrun et al., 2000, 2003; Furlong, 2007), or (ii) the subducted Australian slab is twisted into, and continuous with, the Australian plate boundary beneath the Southern Alps (Sutherland et al., 2000; Reyners et al., 2002).

2-1-2 Tectonic setting of Alpine Fault

The Alpine fault and the South Island, as a whole, evolved from a predominantly translation boundary since ca. 23-22 Ma (Walcott, 1998). Since ca. 20 Ma, the Hikurangi subduction zone has been migrating towards the Puysegur margin. This southward migration led to, both, an increasing amount of transpression in the Alpine Fault (crustal) and the development of the Southern Alps. Over time, the characteristic of the Alpine Fault changed from translational to transpressional, and joined up the northern and the southern subduction zones since ca. 6-10 Ma (Furlong, 2007). The southward migration of Hikurangi also caused the shortening in length of the Alpine Fault plate boundary. The present length of the Alpine plate boundary segment is approximately 60% of the length at 10 Ma (Furlong, 2007).

The Alpine Fault is an intra-continental dextral strike-slip fault which lies adjacent to the Southern Alps. It is a dominant structure in the oblique continental collision between the Australian and the Pacific plates. This plate boundary is observable on land in a zone with a width of approximately 250 km (Lamb, 2011). The converging rate at the Alpine Fault is 35.7 mm/yr for a fault-parallel component, 9.5 mm/yr for a fault-normal component, thus giving a relative plate motion of 37 mm/yr (DeMets et al., 2010). The Alpine Fault is a straight fault zone, expanding over approximately 420 km in length, from Hokitika to Milford Sound (Figure 2-1), whilst exhibiting a thrusting component which results in the uplift of the Southern Alps (Scholz, 1977; Lamb et al., 2015).

Four large faults branched out from the Alpine Fault in the north of Hokitika, namely: Hope Fault; Clarence Fault; Awatere Fault; and Wairau Fault. These four large dextral strike-slip faults make up the Marlborough Fault System (MFS) (Figure 2-1) which transfers motion and displacement between the transform and the Hikurangi Margin. The most active fault, with the highest slip rate, in the MFS is Hope Fault. The fault with with the greatest total displacement in the MFS is Wairau Fault (the westernmost and a direct continuation of the Alpine Fault) since continental crust is caught up in the Alpine-Wairau Faults convergent zone and moved along the MFS (mainly through Wairau Fault) towards the subducted edge of the Hikurangi subduction zone (Walcott, 1998). Through focal mechanism and stress observations, the Alpine Faults seemed to be seismically releasing elastic strain from the

crustal surface down to 10-12 km between the south of Hope Fault all the way down to Milford Sound (Leitner et al., 2001), thus constraining the depth of the straight fault segment.

Southward of the straight segment, the Alpine Fault continues offshore from Milford Sound (Figure 2-1), following the continental margin, until it reaches the Puysegur trench where the strike-slip fault transitions into an eastward-dipping oblique subduction (Lamarche and Lebrun, 2000). The subducted slab (towards NE direction) from the Puysegur subduction zone reaches as far north as Milford Sound where, at depths greater than 40 km, the slab is almost vertical (Leitner et al., 2001).

2-2 Transform Faults

Although this study aims to investigate the evolution process of the whole of New Zealand (2 subduction zones and 1 transform), special attention will also be paid to the continental transform (Alpine Fault) because, as previously mentioned, this will be the first numerical modelling study of the Alpine Fault. Therefore, it is essential to understand the general nature of transform faults and the variety in its occurrence.

2-2-1 Mechanics of Transform Faults

The purpose of a fault is to relieve any strain caused by either extension, compression, or longitudinal stress in the Earth's lithosphere. Transform faults, in particular, relieve the strain built up in regions in-between subduction zones or ridges. Transform fault is a type of strike-slip fault which can be considered as a plate boundary, hence the term transform boundary. At a transform fault, two tectonic plates scrape and slide pass each other. This interaction neither create nor destroy the lithosphere, hence why it is also known as a conservative plate boundary. The relative motions involved in transform setting are mainly in horizontal direction, either dextral (right-handed) or sinistral (left-handed). A noticeable feature of a transform fault is the sudden ending of the displacement, or the changes in form and direction of displacement to a fault which is not truly transcurrent (transverse).

Transform faults are commonly, and not to be, confused with transcurrent fault. Although both types are of strike-slip nature, transform faults end at a junction with a different fault type or plate boundary, while transcurrent faults end with no tectonic continuation. In terms of deformation, transform faults are evenly deform along their segments while transcurrent faults exhibit the greatest deformation in the middle of the fault segment and less so towards the margins.

Transform boundaries do not occur as isolated features, instead, at both ends, they are connected to ridges, subduction zones, or other faults. These form a network of mobile belts, which divides the Earth's surface into several rigid plates (Wilson, 1965). Figure.2-2 is a simplified drawing, illustrating the setting in which transform boundary occurs in nature.

At the points where the transform boundary ends, the horizontally shearing motion along the transform fault is expected to significantly reduce or terminate abruptly (Wilson, 1965; Platt et al., 2008). This reduction of shear motion could arise from features such as the change in motion type, the change in orientation of the boundary, or the transitioning between the

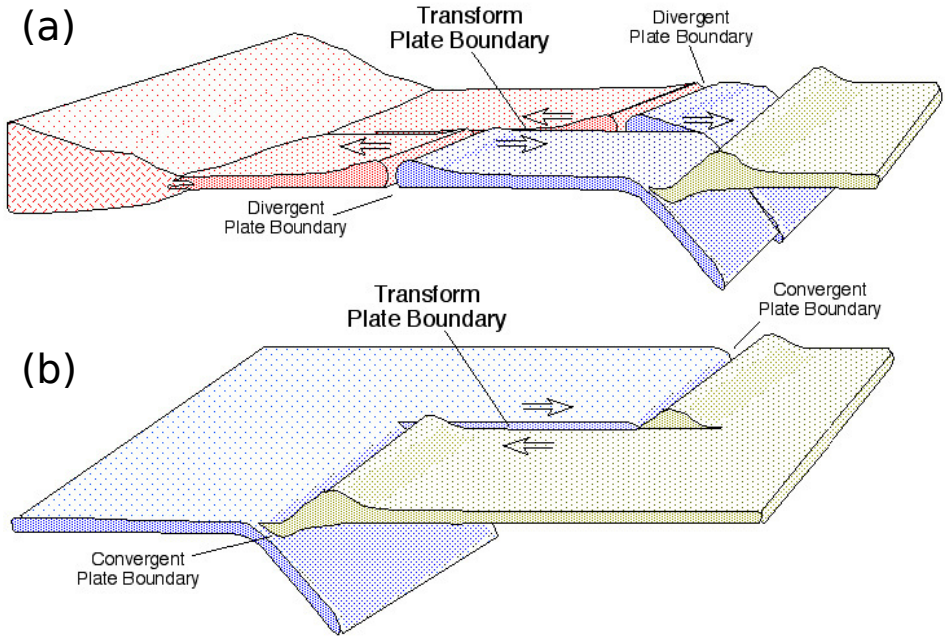

Figure 2-2: Illustrations showing transform plate boundary in two tectonic settings, (a) in-between Divergent plate boundary and (b) in-between Convergent plate boundary (Source: Prof Bruce Railsback, University of Georgia)

continental and oceanic lithosphere. This sharp change of shearing motion is clearer in the case where the transform sits in-between the diverging (spreading centre) plate boundary (Figure 2-2a) e.g. San Andreas Fault Systems. In contrast, when a transform sits in-between two convergent plate boundaries (Figure 2-2b), the shear stress along all of the three plate boundaries could be comparable. A great example of this is the Alpine Fault in New Zealand which sits in-between the Hikurangi and Puysegur subduction zones. Transform faults occur in both oceanic and continental setting, however, this study only focuses on the continental transform since the main focus is on the Alpine Fault of New Zealand.

2-2-2 Continental Transforms

Continental Transforms belong to a group of oblique plate boundaries, from transpressional to transtensional, with gradual transition between them. Transform faults provide a setting which allows the deformation, as a function of temperature and of rock properties, to be studied. Transform fault zones tend to accommodate great tectonic plate motions and crustal deformation, associating these zones with potential natural hazards.

Transform plate boundaries are also zones of highly localised strike-slip shear, extending hundreds of kilometres and accommodating tens to hundreds of kilometres of displacement (Norris and Toy, 2014). The upper 10-15 km of the continental crust deforms in a brittle fashion by shearing motion. This deformation in the seismogenic zone usually leads to a release of seismic energy, associating continental transform boundaries with severe and shallow earthquakes. This prominent seismic activity, as well as the ease of accessibility, makes our

understanding of continental transforms better than that of oceanic transforms'. A review by Norris and Toy (2014) provided an in-depth descriptions of the main continental transforms, as well as the review of the history of numerical studies on the transforms.

Continental transforms can be considered as primarily non-steady state lithospheric fragmentation. Both geophysical observations (Scholz, 1977; Lamarche and Lebrun, 2000; Norris, 2004; Lamb, 2011) data and numerical modelling (Savage et al., 2013) of continental transforms suggest that these systems do not have any long-term steady state. Instead, they evolve continuously due to changes in the lithosphere or rheological structure. The main driving forces behind the evolution of transforms are relative motion of lithospheric blocks, ductile deformation, progressive faulting, and thermal evolution of both the crust and the mantle. The stress distribution and the evolution of material in the surrounding lithospheric rocks, in turn, control the orientation and architecture of continental transforms.

Continental transform faults are typically and dominantly characterised by aseismic creep and generally small ($< 8M_w$) earthquakes. However, records show that larger earthquakes have occurred in the past, which were triggered by factors such as the generation of new transform boundaries or a sudden activation of pre-existing fossil structure.

Several variations exist in the structure and geometry of continental transforms. Brief descriptions of the largest transforms are given as follows: the **San Andreas Fault System** is a large system of, predominantly, strike-slip faults extending approximately 1200 km long, whilst accommodating the right-lateral displacement (50 mm/yr) between the Pacific and the North American plates (Platt et al., 2008). San Andreas exhibits a convergence component in the region of Transverse Ranges ("Big Bend"), where the strike-parallel slip is accommodated (Norris and Toy, 2014); the **North Anatolian** is an active dextral continental transform. Its location signifies the collision zone between both the Arabian, African, and Eurasian Plates, and a boundary between Eurasian and Anatolian Plates; the **Altyn Tagh** is an active strike-slip continental transform, extending 1500 km through northern Turkey. The transform emerged from a collision between the Indian and the Asian plates, which in turn also formed the Tibetan plateau (Norris and Toy, 2014). Its length and displacement is comparable with those of San Andreas'; the **Dead Sea Transform** is a dominantly sinistral strike-slip continental transform. It forms a boundary between the African (Nubian) and Arabian plates; the **Alpine Fault** is a transform inter-linking two subduction zones, it also acts as a plate boundary between the Australian and the Pacific plates. It is recognised as a major strike-slip fault with displacement in the scale of hundreds of kilometres. The faults strike obliquely to the slip vector, giving rise to continental convergence. The regional slip vectors, as well as the development of tectonic complexities, are comparable to those of San Andreas' (Scholz, 1977). These variations give an insight into how their tectonic origins and crustal development and evolution differ (Norris and Toy, 2014).

Chapter 3

Numerical Method

The work in this project was carried out using a 3D thermo-mechanical coupled numerical code, 'I3ELVIS', by Gerya and Yuen (2003, 2007). The code is based on finite-differences numerical schemes. The governing physical laws such as conservation of mass (3-1-1), momentum (3-1-2), and energy (3-1-3), are discretised on a staggered grid (Eulerian). A direct solver is then employed in the solving of the system of linear equations.

A Lagrangian marker-in-cell (Gerya and Yuen, 2003) (also known as marker-and-cell (Harlow and Welch, 1965; McKee et al., 2008)) technique is employed to treat the advection equation. For each time step, the markers are spatially advected with Runge-Kutta scheme. The convergence of the Gauss-Seidel iterative solver is sped up with multi-grid method.

The conservation laws are also coupled with rheology laws. The models in this project specifically employed the visco-plastic rheology, where the viscous rheology is dominated by dislocation creep while the plastic rheology is governed by Mohr-Coulomb failure theory. In this section, brief descriptions of the physicals principles behind the working of the code will be given, as well as the specifics of the model set-up.

3-1 Underlying physical principles

In I3ELVIS, the physical principles implemented in the code are in Lagrangian frame of reference (denoted by $\frac{D}{Dt}$), meaning that we, an observer, follow an individual parcel of quantity as it moves through space and time. Interlinking with Lagrangian view point is the Eulerian frame of reference (denoted by $\frac{\partial}{\partial t}$). In Eulerian view point, an observer stays or focuses on a specific location in space through which the quantity flows as time pass.

This section will provide descriptions of the physical principles behind the working of the code, such as the conservation of mass (3-1-1), momentum (3-1-2), and energy (3-1-3). The physical rock parameters used in this numerical study are given in Table 3-1.

3-1-1 Conservation of Mass (Continuity Equation)

The conservation of mass can be mathematically expressed in a differential form as the continuity equation (3-1-1.1), where ρ is density, t is time, and $\vec{v}$ is the flow velocity vector field. Since the quantity of mass is extensive (additive for systems) and is related to the intensive (bulk property) quantity of density(ρ), therefore the density is used in the continuity equation.

$$\frac{\partial \rho}{\partial t} + \nabla \cdot (\vec{v}\rho) = 0 \tag{3-1-1.1}$$

In fluid mechanics, the continuity equation states that, in a steady-state system, mass leaves a system at the same rate as at which mass enters the system. Equation 3-1-1.2 shows the Lagrangian time derivative form of the continuity equation, with $\frac{D\rho}{Dt} = \frac{\partial \rho}{\partial t} + \vec{v} \cdot \nabla \rho$.

$$\frac{D\rho}{Dt} + \rho(\nabla \cdot \vec{v}) = 0 \tag{3-1-1.2}$$

If there is a change in density over time, this would mean that our media is either compressed or expanded, resulting in a change in mass which is prohibited. Therefore, the mass conservation law requires $\frac{D\rho}{Dt} = 0$, leading to $\nabla \cdot \vec{v} = 0$, i.e. incompressible flow fields assumption. Although a strong assumption and simplification, the incompressible continuity equation is still widely implemented in geodynamical numerical modelling.

3-1-2 Conservation of Momentum (Navier-Stokes Equations)

In the law of momentum conservation, the intensive quantity is a product of density and velocity vector field, $\rho\vec{v}$, and the extensive quantity is a product of mass and velocity vector, $m\vec{v}$.

$$\frac{\partial \vec{v}}{\partial t} + \vec{v} \cdot \nabla \vec{v} = \vec{f^e} + \frac{1}{\rho}\nabla \cdot \sigma \tag{3-1-2.1}$$

Equation 3-1-2.1 is the general expression for the Momentum Conservation Law, where $\frac{\partial \vec{v}}{\partial t}$ is the inertial term, $\vec{v} \cdot \nabla \vec{v}$ is expressing convective acceleration, $\vec{f^e}$ expresses the body force (gravity, $\vec{g}$), and the term $\frac{1}{\rho}\nabla \cdot \sigma$ represents surface forces where σ is the strain rate.

In the case of viscous fluid (Newtonian fluid), consider $\sigma = -P\mathbf{I} + \mu\nabla\vec{v}$, where P denotes pressure, $\mathbf{I}$ is an identity matrix, and μ denotes viscosity. With this consideration, the Navier-Stokes is expressed as equation 3-1-2.2, where $\nu = \frac{\mu}{\rho}$ denotes kinematic viscosity.

$$\begin{aligned} \frac{\partial \vec{v}}{\partial t} + \vec{v} \cdot \nabla \vec{v} &= \vec{g} + \frac{1}{\rho}\nabla \cdot (-P + \mu\nabla\vec{v}) \\ \frac{D\vec{v}}{Dt} &= \vec{g} - \frac{1}{\rho}\nabla P + \nu\nabla^2\vec{v} \\ \rho\frac{D\vec{v}}{Dt} &= \rho\vec{g} - \nabla P + \rho\nu\nabla^2\vec{v} \end{aligned} \tag{3-1-2.2}$$

In flows with high viscosity, the inertial forces ($\frac{D\vec{v}}{Dt}$) becomes much smaller than the body (gravitational) force, and therefore is negligible, which leads to the expression 3-1-2.3.

$$\rho\vec{g} - \nabla P + \rho\nu\nabla^2\vec{v} = 0 \tag{3-1-2.3}$$

$$\rho\nu\nabla^2\vec{v} - \nabla P = -\rho(T, P, c)\vec{g} \tag{3-1-2.4}$$

In the numerical modelling of fluid dynamics, the fluid temperature is allowed to vary from one position to another, driving the fluid flow. This also allows the Boussinesq approximation to be imposed onto our buoyancy-driven flow problem. The approximation only takes the density difference that is multiplied by gravity into consideration, and the rest is assumed to be constant. This is because in the buoyancy force term, the temperature and volatile content play vital parts. Therefore, the density in buoyancy force term, $\rho\vec{g}$, is allowed to be varied locally as a function of temperature (T), pressure(P), and composition (c), leading to the final form in equation 3-1-2.4.

3-1-3 Conservation of Energy (Heat Transport Equation)

Heat transport equation arose from the law of energy conservation under the consideration of slowly moving system or external work with the 'energy' being a product between specific heat (C_p) and temperature (T). A few assumptions are also in place: (i) C_p is constant; and (ii) mass conservation equals zero. Thus, the obtained Lagrangian heat transport equation reads the following,

$$\rho C_p \frac{DT}{Dt} = \nabla \cdot (k\nabla T) + \underline{q}_H \tag{3-1-3.1}$$

where k denotes thermal conductivity, which is a function of temperature, pressure, and composition, i.e. $k(T, P, c)$, while $\underline{q}_H$ denotes heat sources. In geodynamical processes, the considered heat sources are radioactive heat (H_r), adiabatic heat (H_a), latent heat (H_L), and shear heat (H_s), leading to equation 3-1-3.2,

$$\rho C_p \frac{DT}{Dt} = \nabla \cdot (k\nabla T) + H_r + H_a + H_L + H_s \tag{3-1-3.2}$$

where,

$$H_r = constant \tag{3-1-3.3a}$$

$$H_a = T\alpha\vec{v}\nabla P \tag{3-1-3.3b}$$

$$H_L = constant \tag{3-1-3.3c}$$

$$H_s = \sigma_{ij}(\dot{\varepsilon}_{ij} - \dot{\varepsilon}_{ij(elastic)}) \tag{3-1-3.3d}$$

In adiabatic heat source (H_a), T denotes temperature in Kelvin and α denotes thermal expansion. The shear heat (H_s) is composed of components of the deviatoric stress tensor (σ_{ij}) and deviatoric strain rates ($\dot{\varepsilon}_{ij}$). This shows that the conservation laws is coupled with rheology laws (3-1-4) through the deviatoric strain rate ($\dot{\varepsilon}_{ij}$). The combination of the set of equations 3-1-3.3 and equation 3-1-2.4, together, form the Extended Boussinesq Approximations.

3-1-4 Rheological constitutive equations

As mentioned in the beginning of Chapter 3, the conservative laws are coupled with rheology law. More specifically, I3ELVIS employs the a visco-elasto-plastic rheology, with the deviatoric strain rate ($\dot{\varepsilon}_{ij}$) being composed of three components, i.e.

$$\dot{\varepsilon}_{ij} = \dot{\varepsilon}_{ij(viscous)} + \dot{\varepsilon}_{ij(elastic)} + \dot{\varepsilon}_{ij(plastic)}, \tag{3-1-4.1}$$

where

$$\dot{\varepsilon}_{ij(viscous)} = \frac{1}{2\eta}\sigma_{ij} \tag{3-1-4.2a}$$

$$\dot{\varepsilon}_{ij(elastic)} = \frac{1}{2\mu}\frac{D\sigma_{ij}}{Dt} \tag{3-1-4.2b}$$

$$\dot{\varepsilon}_{ij(plastic)} = \begin{cases} 0, & \text{for } \sigma_{\mathrm{II}} < \sigma_{yield} \\ \chi\frac{\partial G}{\partial \sigma_{ij}} = \chi\frac{\sigma_{ij}}{2\sigma_{\mathrm{II}}}, & \text{for } \sigma_{\mathrm{II}} = \sigma_{yield} = G. \end{cases} \tag{3-1-4.2c}$$

From the equations 3-1-4.2, η denotes the viscosity, σ_{ij} denoted the deviatoric stress component, σ_{yield} is the plastic yield strength of a given rock, σ_{II} denoted the second deviatoric stress invariant, and χ denoted the plastic potential.

3-2 Model Setup

The experimental setup in this investigation aims to model the geodynamical processes in the upper mantle and the corresponding development in the lithospheric crust. The 3D numerical model box is shown in Figure.3-1. The model box has physical dimensions of 1500 km (X-axis) × 200 km (Y-axis) × 1200 km (Z-axis), and within it, contained 501 × 101 × 405 uniformly distributed nodes.

The boundary condition allows for free-slip on faces $x = 0$ and $x = L_x$. The composition layers in the model box is arranged as the following: 'sticky air'[1] (y= 0-15 km); oceanic crust (15-23 km); continental crust (12-47 km); lithospheric mantle (Moho to 105 km); and asthenospheric mantle (105-200 km). The Moho depth is 8 km under oceanic crust and 35 km under continental crust, from crustal surface. The weak-zones make an angle of 63.4° to the vertical plane.

3-2-1 Seed (weak-zone) Placements

Each pair of models has the same weak zone configurations. Some pair of models have greater curvature, but essentially there are 3 main sections of the prescribed weak-zones (Figure.3-1).

1. **Northern Segment** is to emulate the Hikurangi subduction zone. The prescribed weak zone is dipping to the west (the left side of the model box) in order to allow the Pacific plate to subduct under the Australian plate.

[1] low density (1 kg/m^3) and high viscosity (10^{18} Pa·s) material. This viscosity is sufficiently lower than lithospheric rocks.

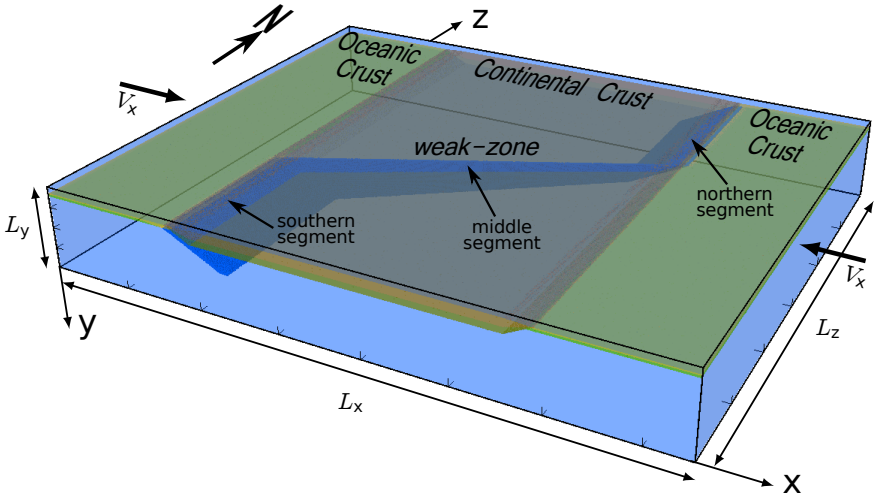

Figure 3-1: A 3D model box used in the investigation. The dimensions of the model box are $(L_x, L_y, L_z) = (1500,200,1200)$ km. The blue planes represent the prescribed weak-zones. The green thin slab represent the oceanic crust. The thicker slab in the middle (implemented in the middle) is the continental crust. The velocity ($V_x = 37.8$ mm/yr) is directed inwards from both ends of L_x.

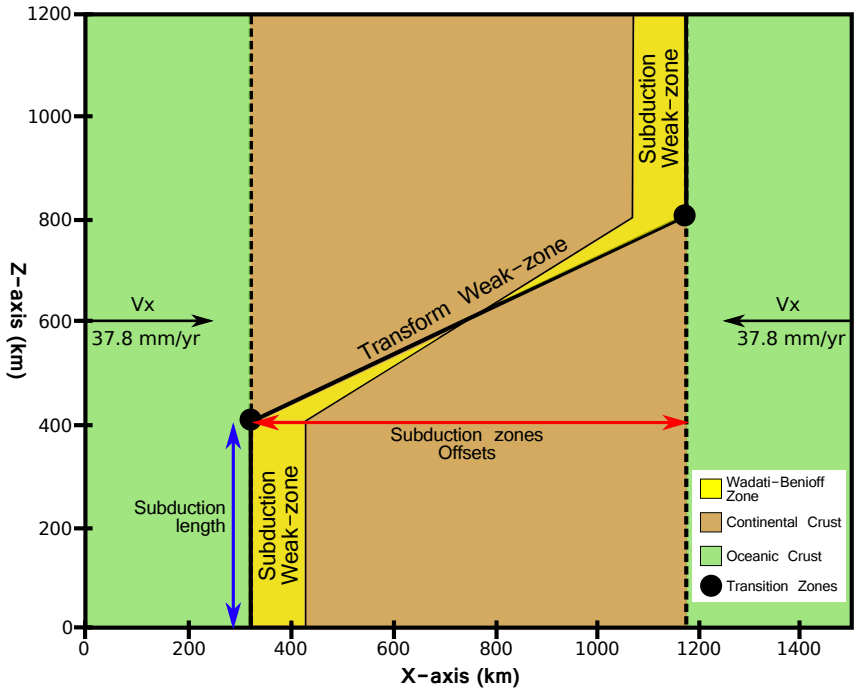

Figure 3-2: Detailed configuration of the model box (XZ–plane). The constructed models involve varying factors such as the implementation of continental crust (Set 1), subduction zones lengths (Set 2), subduction zones offsets (Set 3), or the presence of transform weak-zone (Set 2 and 3). The transition zones refer to the region connecting the subduction zone to the transform. Note: the Wadati-Banioff zones are for representative purpose only and is not to scale.

2. **Middle Segment** is to emulate the continental transform boundary, the Alpine Fault. This segment is linking the two subduction zones together. Due to the symmetry between the two subduction weak-zones, in some sets of models, this linking segment will have a twist (change in dipping direction) in the middle of the segment.

3. **Southern Segment** is to emulate the Puysegur subduction zone, which is dipping to the east (the right side of the model box) to allow the Australian plate to subduct under the Pacific plate.

The width of the continental crust is adjusted from model to model according to the subduction zones offset. The rheology and rock compositions of all the Earth's layers, including the prescribed weak-zones, are from Ranalli (1995) (Table 3-2). The Felsic crust rheology is assigned to both the Upper Continental Crust and the Lower Continental Crust. The Upper Oceanic Crust is prescribed with Basalts crust, and the Lower Oceanic Crust is prescribed with Gabro rock type. As for the weak-zones, the prescribed rheology is dry mantle Peridotite, as well as crustal Basalts.

3-3 Experimental Model Plans

This investigation comprises four sets of models. Each set allows us to study the influence of different model geometry on the tectonic evolution.

The first set of models (Table 3-2) consists of four pairs (kita-kitf). This set of models aims to explore any general characteristics that could arise from basic geometry weak-zones. In this set, the each pair have one model with oceanic-oceanic crustal features, while another has oceanic-continental-oceanic crustal features (Figure 3-1, 3-2).

The second set of models consists of three models, namely kitg, kith, and kiti (Table.3-2). These models contain only the subduction weak-zones segments and no transform weak-zone. The subduction offsets are kept constant at 900 km (therefore, so is the width of the continental crust), while the subduction length (in Z-axis) varies. All of the models have oceanic-continental-oceanic crustal features. This set of models aims to investigate how the transitional zone might naturally develops.

The third set of models consists of three models, namely kitj, kitk, and kitl (Table.3-2). Similar to the second set of models, the models in this set have no transform weak-zone. All of the models in this set have oceanic-continental-oceanic crustal features. The subduction length is kept constant at 400 km. The subduction zones offsets, and therefore the width of continental crust, is allowed to vary. The purpose of this set of model is to experiment with different offsets between the two subduction zones, and how the transform zone may naturally develop (according to the simulation).

The fourth set comprises only one model, kitm. The entire length of the transform weak-zone in this setup dips in the north-west direction. The subduction length is 400 km, and the subduction zones offset is 900 km. This model setup allows us to investigate the influence of one-sided collision transform has on the tectonic evolution, as oppose to other setups which are symmetrical.

Table 3-1: The physical rock parameters implemented in the numerical modelling.

Physical Properties	Continental Crust		Oceanic Crust		Mantle	
	Upper	Lower	Upper	Lower	LITH[a]	ASTEN[b]
Rheology	Wet Quartize	Wet Quartize	Basalt	Gabro	Dry Olivine	Dry Olivine
Pre-exponential factor (A) $[Pa^n s]$	1.97e+17	4.80e+22	4.80e+22	4.80e+22	–3.50e+22	–3.50e+22
Exponent in flow law (n) $[Power]$	2.3	3.2	3.2	3.2	3.5	3.5
Activation Energy (E_a) $[J]$	1.54e+05	2.38e+05	2.38e+05	2.38e+05	5.40e+05	5.40e+05
Activation Volume (E_v) $[J/bar]$	0	0	0	0	1.7	1.7
Critical Stress (σ_{crit}) $[Pa]$	3.00e+04	3.00e+04	3.00e+04	3.00e+04	3.00e+05	3.00e+05
Density (ρ) $[kg/m^3]$	2750	3000	3000	3000	3300	3300
Thermal Conductivity (κ_t) $[m \cdot K]$	0.64	1.18	1.18	1.18	0.73	0.73
Radioactive Heating (H_r) $[W/m]$	2.00e–06	2.00e–07	2.20e–07	2.40e–07	2.20e–08	2.20e–08

[a] Lithospheric Mantle (Moho – 100 km), The Moho depth is 8 km under oceanic crust and 35 km under continental crust, from the crustal surface.
[b] Asthenospheric Mantle (100 – 200 km)

Table 3-2: Model Plan

Models	Crustal Features[a]	Subduction Zone length (km)	Subduction Zones Offset (km)	Prescribed Transform Weak-Zone
Reference Model				
kitd[b]	OC	400	900	Yes[c]
Set 1: Oceanic-Oceanic vs Oceanic-Continental Subduction				
kita	OO	400	900	Yes[c]
kitb	OC	400	900	Yes[c]
kitc	OO	400	900	Yes[c]
kite	OO	400	900	Yes[c]
kitf	OC	400	900	Yes[c]
Set 2: Influence of subduction-zone lengths[d]				
kitg	OC	500	900	No
kith	OC	400	900	No
kiti	OC	300	900	No
Set 3: Influence of subduction-zone offsets[e]				
kitj	OC	400	300	No
kitk	OC	400	500	No
kitl	OC	400	700	No
Set 4: The entire transform weak-zone dips NW				
kitm	OC	400	900	Yes[f]

[a] OO: Oceanic-Oceanic, OC: Oceanic-Continental subduction.
[b] kitd also belongs to Set 1.
[c] two-sided collision transform.
[d] Refer to the red line in Figure 3-2.
[e] Refer to the blue line in Figure 3-2.
[f] one-sided collision transform.

Chapter 4

Results

4-1 Reference Model

The model kitd, whose evolution is shown in Figure 4-1, is selected to be the reference model since its physical responses gave rise to features comparable to natural observations to an extent. The reference model also represents the two-sided collision transform (weak-zone) setup.

4-1-1 Development at the subduction zones

At the two subduction zones, the oceanic crusts subduct under the continental crust, along the plane of the prescribed weak zones. Since the weak-zone is implemented on the edge of the continental crust, the incoming oceanic crusts subduct without splitting the upper and lower continental crusts. This is illustrated through the visualisation of rock compositions, Figure 4-1.

Both subduction zones develop (migrate) towards the transform. This means that the northern subduction zone develop towards the SSW direction while the southern subduction zone develops in the NNE direction. In order to illustrate this, we look specifically at the northern subduction zone. The plates subduction occurs at different time at different position. From z=900 km to z=1200 km, the plate subduction initiated at around 0.7 Myr. As the evolution proceeded, subduction at z=800 km are observed after 1.5 Myr, and at the centre of the transform (z=600 km) after 5 Myr.

As subduction proceeds, there seems to be an insignificant amount of thickening of continental crust. This is illustrated through the composition visualisations, where the continental crust appears to be pushed by the subduction but not a great deal of crustal thickening is happening. The stress imposed on the continental crust from the subduction resulted in some uplift on the surface. This can be clearly observed in the topographic plots (Figure 4-3a), where the fore-arc regions exhibit distinctively higher topography than the surrounding areas. Some features observed through the visualisation of viscosity (Figure 4-2 (left and right columns)) could potentially suggest the occurrence of accretion wedges in the fore-arc regions.

4-1-2 Development at the transition zones

In the transition zones (z=300 – 400 km and z=760 – 900 km), the implemented weak zones sit beneath the continental crust (not at the edge). As the oceanic plate pushes in, a fraction of the lower continental crust are pushed down (in y-axis) along the prescribed weak zone. This is illustrated by the composition cross-sections at z=375 km and 825 km (Figure 4-1a and b). By 1 Myr, the subducting oceanic crust has already pushed a small fraction of the lower continental crust down towards the mantle. At around the same time, the untorn lower continental crust in the fore-are region appear to have intruded upwards into the upper continental crust. This upward shearing are also observable in the viscosity and strain-rate cross-sections. Around 2 Myr, Figure 4-1b, the cross-section of composition at the transition zone also exhibits slab-tearing (zoomed area in Figure 4-1b) of the sinking lower continental slab.

4-1-3 Development at the transform

In the centre of the transform (around z=600 km), the viscosity visualisations show a clear structure of the two-sided continental-continental collision (Figure 4-2b,e,h,k,n, and q). On the flanks of the continental crust, comb-shaped regions of low viscosity ($10^{22} - 10^{23}$ Pa·s) is observed in the region of high viscosity (10^{24} Pa·s). These similar features are observed as regions of intermediately high strain-rate (-16 to -15 s^{-1}) in the strain-rate visualisations. These features, therefore, appear to signify regions of sequential faulting. The fault-like structures are observed at the base of the oceanic crusts and could potentially be extending into the upper mantle, i.e. from y=15 km to 25 km (Figure 4-2e and h). These fault-like structures disappear after 5 – 6 Myr, when the migration of subduction zones reaches the centre of the transform.

Also at the centre of the transform, the thickening and the shortening of the continental crust (Figure 4-1) occurred up to 4 Myr, after which the upper and lower continental crusts separated out. This is well illustrated in the composition cross-sections. We can observe that the orientation of the oceanic plates' motion remained almost purely lateral up to 2 Myr, after which the oblique components from the subduction zones caused the oceanic plates to deviate downwards (in y-axis), as illustrated in the zoomed region in Figure 4-1d. At around 4 Myr (Figure 4-1c), the composition cross-section of the centre of the transform shows that the continental crust have significantly shorten and thicken, to the point where the incoming oceanic crust are pushing in at the middle of this thickened continental crust. This motion, aimed at the middle of the continental crustal unit, initiated the separating of the upper and the lower continental crusts. After 4.5 Myr, the upper continental crust spread over and override the subducting oceanic crust (Figure 4-1d). The lower continental crust, however, are still being pushed in and dragged down by the subducting oceanic crust, continuing the crustal thickening and shortening (Figure 4-1e and f.)

4-1-4 Topographic development

The surface expression of the model kitd exhibits a very symmetrical features, i.e. the topographic development in the northern/eastern half is mirrored in the southern/western half.

The noticeably high topography is observed along the plane behind the fore-arcs (on the continental crust), at the transition zones, and the transform (after 0.5 Myr). The areas with the highest bathymetry are the trenches, formed in the subduction zones, on the oceanic crust. The high topography in the fore-arc regions and the region over the transform jointly developed between $0.5 - 2.5$ Myr (Figure 4-3b). After 2.5 Myr, the high topography regions separated out and evolved separately (Figure 4-3c). The continental crust began with a topography of around $3 - 4$ km, and by 5 Myr the flat plain of the continental crust has been uplifted to a topography greater than 5 km (Figure 4-3d,e,and f).

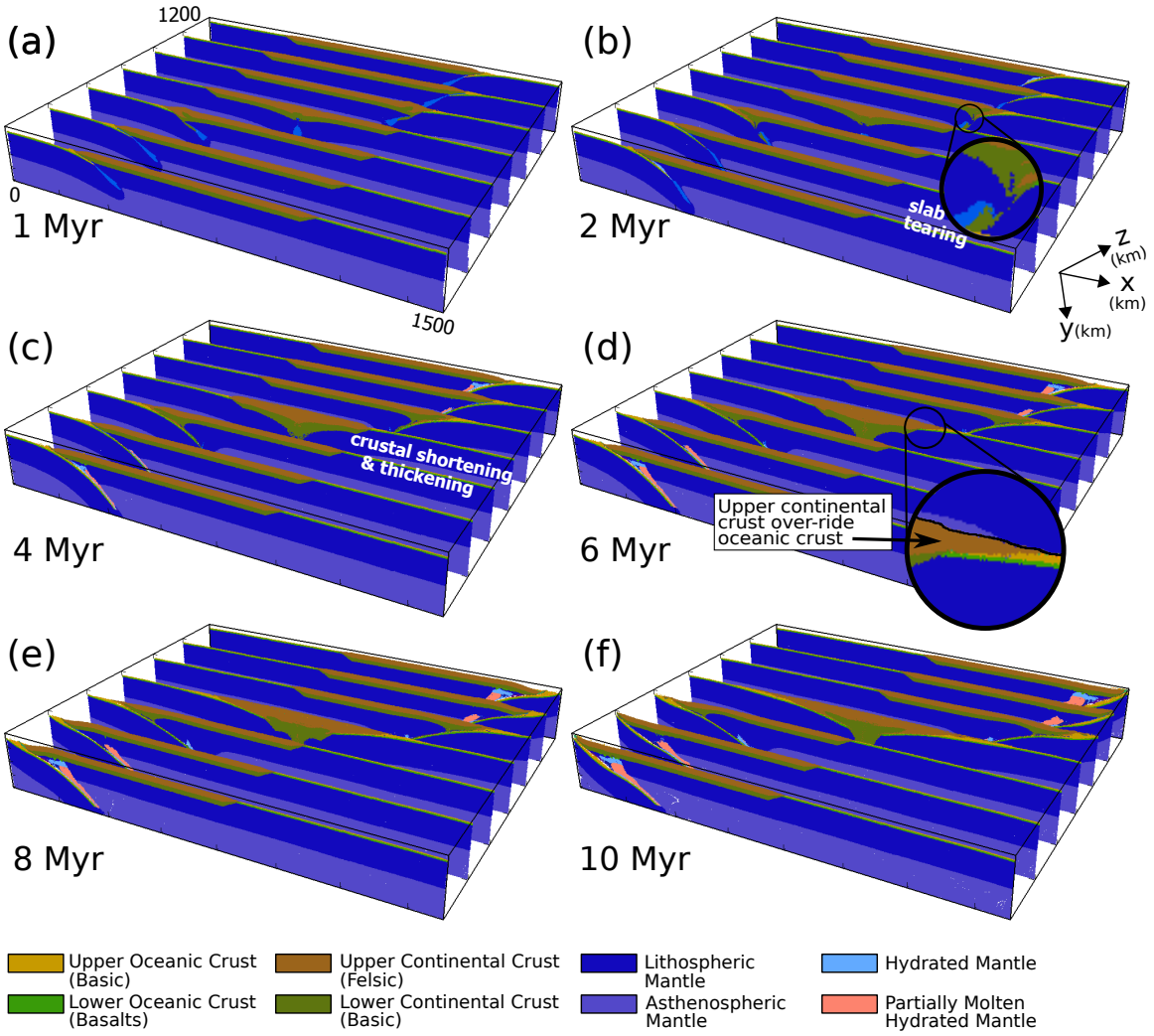

Figure 4-1: The composition evolution of the reference model (kitd). The reference model comprises two-sided collision transform weak-zone setup. The cross-sections are dissected from every 200 km along the z-axis. The evolution of the transform exhibit significant amount of crustal thickening. The zoomed-in region at 2 Myr (b) is from the transition zone (the joining point between subduction zone and the transform), which shows slab-tearing of the lower continental crust. The zoomed-in region around 6 Myr (d) signifies the instance at which only the lower continental crust continues to shorten and thicken, while the the upper continental crust overrides and spreads outwards onto the oceanic crust.

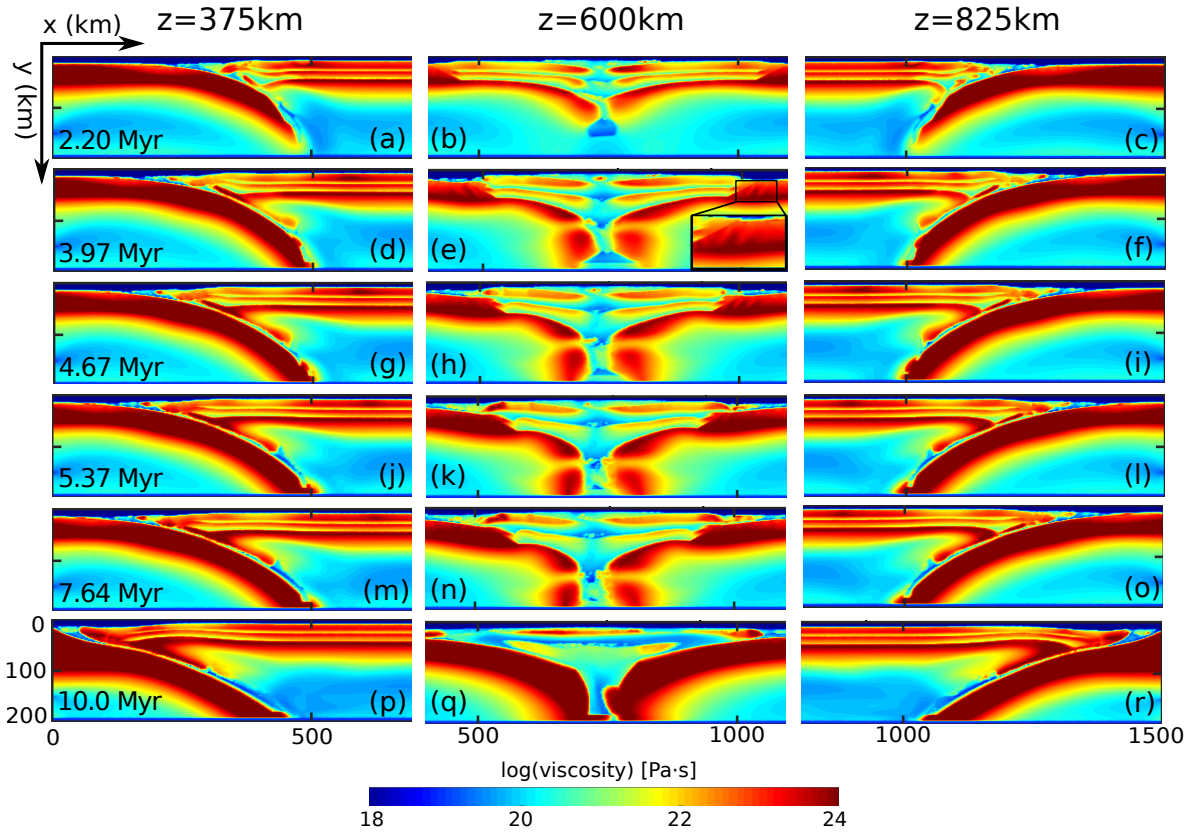

Figure 4-2: The viscosity evolution of the reference model, kitd. The left column displays the viscosity cross-sections at z=375 km (a,d,g,j,m,p), the representation of Puysegur subduction zone (southern). The middle column (b,e,h,k,n,q) are cross-sections from z=600 km, representing the centre of the transform (Alpine Fault). The cross-sections in the right column (c,f,i,l,o,r) are dissected from z=825 km, and represent the Hikurangi subduction zone (northern). The enlarged area, shown in (e), shows faulting-like features in the upper lithospheric mantle which, in turn, reflects how the area responds stress/compression. The centre of the transform (b,e,h,k,n,q) shown here are viewed obliquely to the transform, which make the structure appear to be 2-sided subduction. However, the two plates collide and move obliquely, relatively to one another.

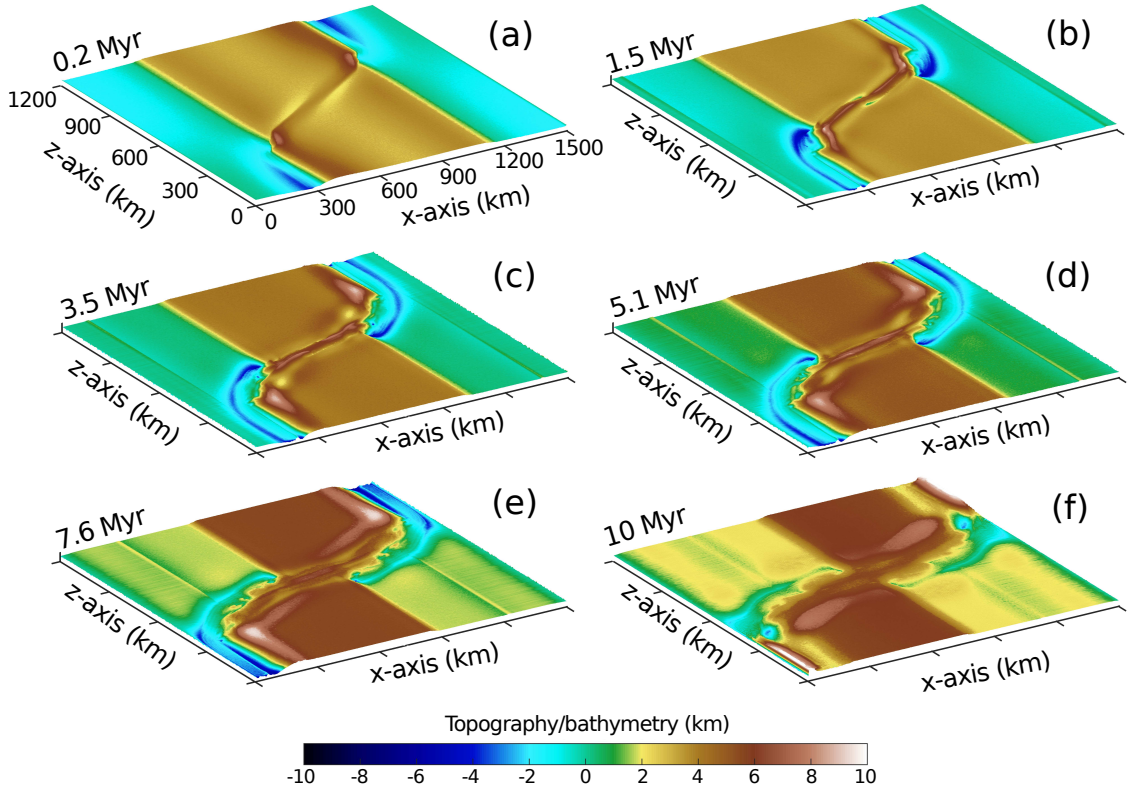

Figure 4-3: A collection Figures showing the topographic evolution of the reference model (kitd). The developed topography shows simple geometry. The highest topography localised in 3 main segments, next to the 2 subduction zones and along the transform. However, this pattern persists up to around 7.6 Myr (e), after which the majority of the nothern- and southern-half of continental plate starts to make less contact with one another.

4-2 Influence of Continental Crust

Set 1 models (Table 3-2) were constructed so that the difference in tectonic evolution can be compared between the models with oceanic-oceanic (OO) subduction (kita, kitc, and kite) and ones with oceanic-continental (OC) subduction (kitb, kitd, and kitf). The results of Set 1 models shows the importance of implementing continental crust in the model. Figure 4-4 shows a comparison between OO and OC model setups.

Composition visualisations of the subduction zones are shown in Figure 4-4 (a1, a3, a4, and a6). The general subduction activity are very similar for both types of model setups. The noticeable difference is the amount of the upper oceanic crust, in the down-going slab, being held back. The models with continental crust scrape or hold back a greater amount of the upper oceanic crust than the models with oceanic-oceanic subduction. This could be due to the fact that continental crust is thicker, therefore asserting more force at the convergent zones. This feature is well illustrated in the case of kitb (Figure 4-4a1) where the continental crust scrapes a great amount of material from the subducting oceanic crust. In contrast, the non-subducting oceanic crust in oceanic-oceanic model setup (Figure 4-4a4) does not hold back as much material as in the case of oceanic-continental model setup.

Figure 4-5 displays the comparison of the strain-rate between the models with (b) and without (a) continental crust. At the subduction zones, the strain-rate of the two model setups shows similar general characteristics. The highest strain-rates, i.e. the highest deformation rate, are localised in the faulting planes.

High topography is expected along the transform boundary (as this would be the Southern Alps). This feature is present in the case of oceanic-continental model setup (Figure 4-4b) but is significantly lacking in the case of oceanic-oceanic model setup (Figure 4-4c).

The composition cross-sections from oceanic-continental model setup (Figure 4-4a2) displays (continental) crustal thickening in the (lateral) centre of the transform. The cross-section of kita (Figure 4-4a5) displays the oceanic crust separated in the centre, due to the centre of transform being twisted (i.e. change in subducting direction).

Comparing the strain-rate of at the transform (Figure 4-5), it is clear that the structures of the transform differ between the two setups. Firstly, the model with continental crust have a wider (x-z view) area of high strain-rate, as oppose to a narrow and well-localised strain-rate in the models with no continental crust. Secondly, from the x-y cross-sections, we can observe layers of high strain-rate within the continental crust itself, whereas in the oceanic-oceanic subduction models, there is only a narrow and localised region of high strain-rate. The layers of high strain-rate in oceanic-continental model setup could arise from the separation of the upper and the lower continental crust as the system evolves.

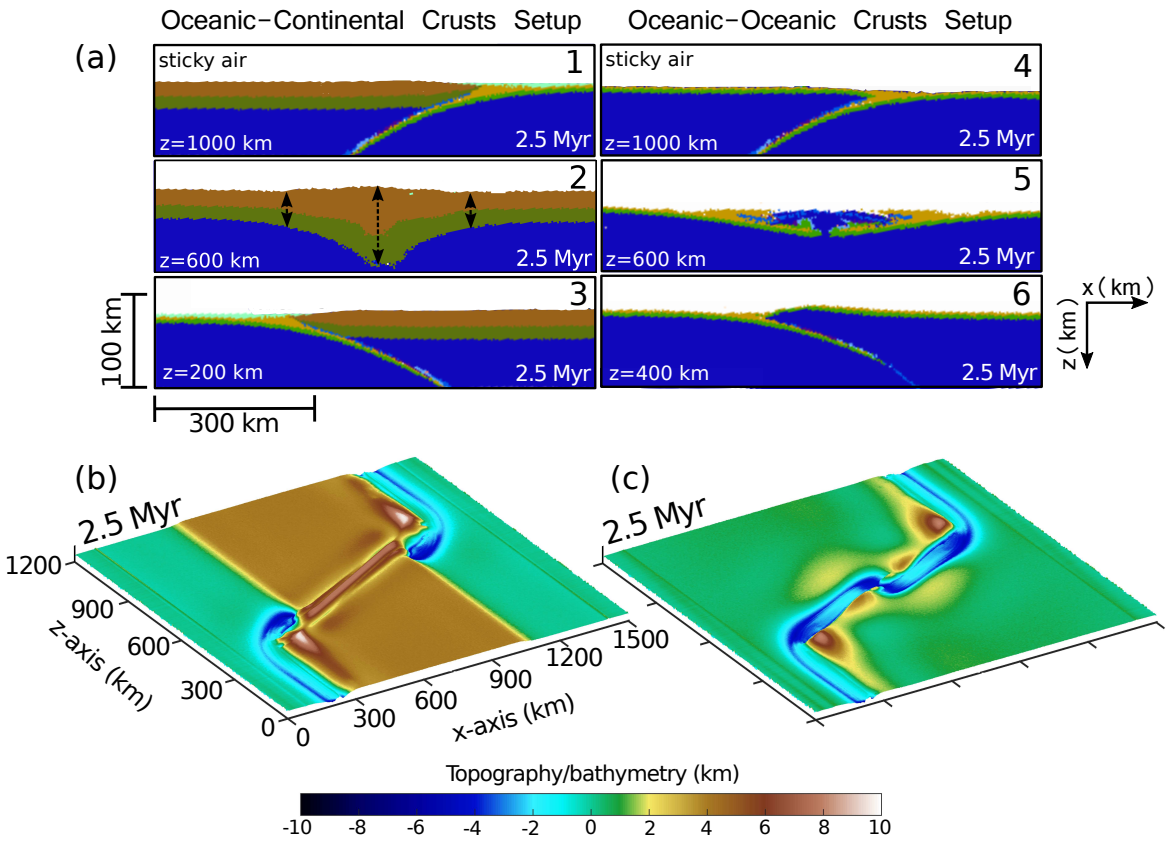

Figure 4-4: Composition and topography/bathymetry visualisations to compare between oceanic-continental crustal setup (a(1,2,3), b) and oceanic-oceanic crustal setup (a(4,5,6),c). The composition cross-sections illustrate that the models which are implemented with continental crust produce features with greater potential to be compared to nature.

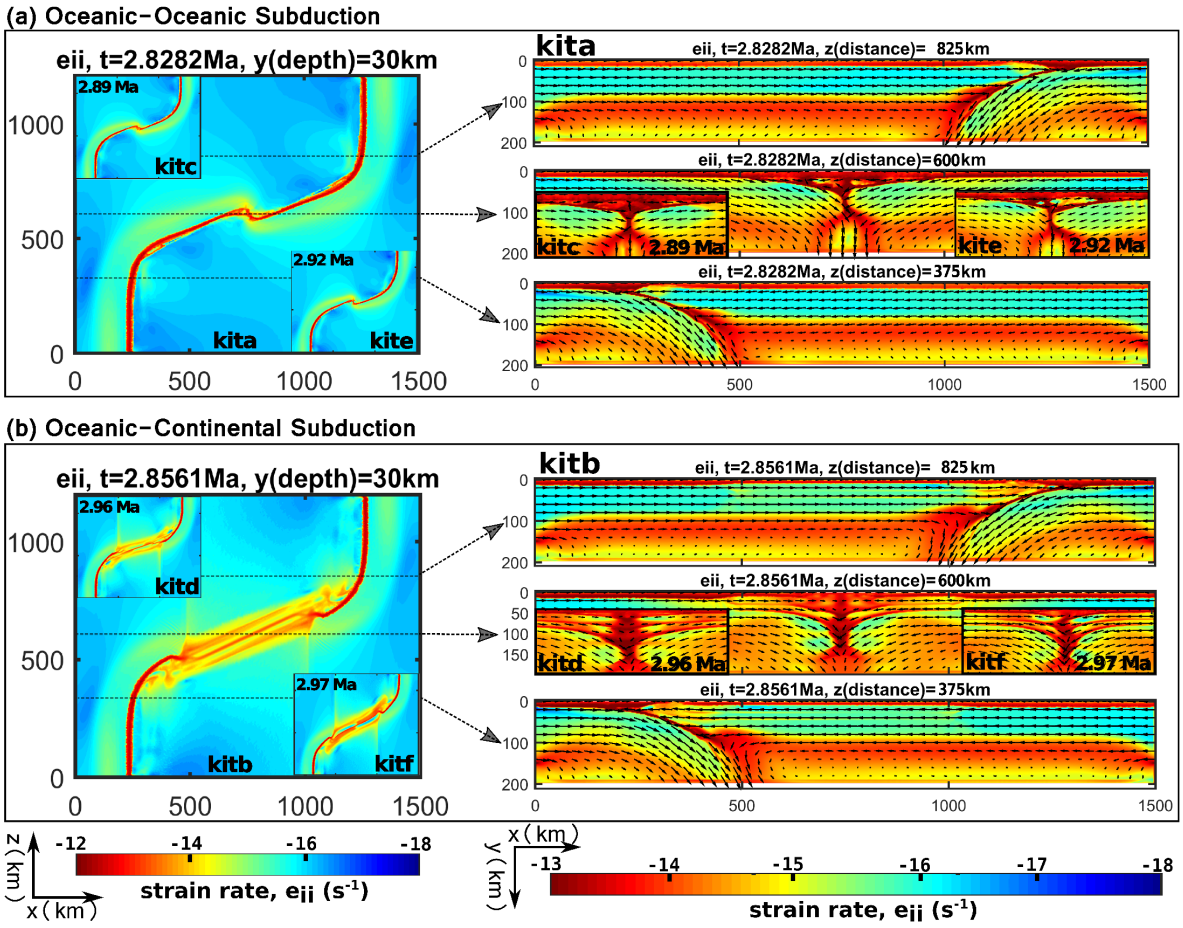

Figure 4-5: Strain-rate visualisations of models with oceanic-oceanic subduction models (kita,kitc, and kite) and the oceanic-continental subduction models (kitb,kitd, and kitf). The general characteristics of the observed strain-rate are similar among the models from each model setup. The high strain-rate regions are localised in the faulting zones i.e. along the subduction zones and the transform. Even though each pair of models initially had weak zones of different curvature, over time, a similar outline of high strain-rate regions are observed.

4-3 Influence of Subduction Zones Geometry

Two additional sets of models were constructed in order to explore the influence the subduction zones geometry on the evolution of the whole system. Set 2 (Table 3-2) is composed of three models (kitg, kith, and kiti) with different subduction length (500 km, 400 km, and 300 km respectively). Set 3 (Table 3-2) is also composed of three models (kitj, kitk, and kitk) with different subduction zones offset (300 km, 500 km, and 700 km respectively). Also, there is no prescribed weak zones in the transform section in any of these models. This also allows us to explore the 'natural' development of the transform region.

4-3-1 Variation of subduction length

The visualisations of Set 2 Models are shown in Appendix A. The 500km-long subduction zones in kitg resulted in a narrow (in z-axis) transform zone. The narrow transform zone of kitg's, therefore, has the smallest oblique-motion components compared to the case of kith and kiti. This also leads to the transition zone (between the transform and the subduction zones) in kitg exhibiting a limited amount of crustal thickening. However, some uplifted areas are observable on the continental plate, as a way of accommodating the compressional stress at the subduction margins.

A shorter distance (in z-axis) between the two subduction zones in kitg also means there is a smaller volume to accommodate the stress as the two sides are pushing in on each other, therefore, a weak-zone developed as a localised straight segment. This straight transform allows the continents to converge with lower obliquity than other models in this set. This is illustrated through the strain-rate visualisations (Figure A-4, A-6, and A-8) where the strain-rate in the cross-section at z=600 km shows that the strain-rate in kitg is localised in the shallower depth than the other two models. This feature is confirmed by the visualisation of material compositions (Figure A-2), as well as the viscosity visualisations (Figure A-5, A-7, and A-9), where the root of the transform structure in kitg appears to reach a depth less than 100 km, whereas kiti's transform root reaches a depth greater than 120 km.

Figure A-1 displays the topographic and bathymetric evolution of Set 2 models. For the surface expression, kitg develops a simple straight uplifted segment, while kith and kiti exhibit somewhat sinusoidal-looking features. By 4.5 Myr, while the topography/bathemetry in kitg still remains a simple straight segment as before, the surface expression of kith and kiti has increased in their complexity, forming features resembling mountain peaks and valleys.

4-3-2 With vs Without Transform Weak-Zone

The model kith (from Set 2) represents the model setup without a prescribed transform weak-zone, which can be compared with the reference model (kitd) to study how the whole system evolves with and without the prescribed transform weak-zones. Despite having no prescribed transform weak-zone, the 3D structures of the model (kith) still manage to evolve in a similar manner as in the reference model. Figure 4-6 compares the material compositions (a and b), strain-rate (c and d), and viscosity (e and f) of the two models at the age of 4.5 Myr. Their subduction zone structures exhibit similar characteristics. The key differences lie in the transform. The composition slices (Figure 4-6a and b) shows that, at the centre

of the transform, kitd exhibits a greater amount of crustal thickening, specifically the lower continental crust, than kith. This is due to kitd having a prescribed weak-zone, which allows for the crustal materials to sink down the prescribed path, and together with the compressional force from both subduction zones, giving rise to a thicker continental crust at the centre of the transform. The thicker crustal structure in the reference model (Z=600 km) is further confirmed by the strain-rate visualisations (Figure 4-6c and d), where the layers of high strain-rate (between the continental layers) in no-transform model is localised at a shallower depth than in the reference model. The viscosity visualisation (Figure 4-6(e and f)) also shows that, at 4.5 Myr, the upper mantle (high-viscosity slabs) in the reference model are at a greater depth than those in the model without transform weak-zone.

Another interesting observation to note is the region at the top of the upper continental crust in the viscosity cross-sections, Figure 4-6e and f. The top of the continental crust (centred around x=750 km) in kith exhibits a distinct and highly viscous segment (Figure 4-6f), which is not present in the case of the reference model (Figure 4-6e). A plausible explanation for this could, again, be the fact that the reference model has a prescribed weak-zone, so when the central transform is compressed by the subduction on both sides, the materials sink down in order to compensate for the built-up compression. However, this is not the case for the model without a transform weak-zone, as when the continental transform is compressed, there is no single assigned pathway for the material to relieve the stress, hence the top segment at the centre appear to be underthrusted by the sandwiching upper continental layers (Figure 4-6f).

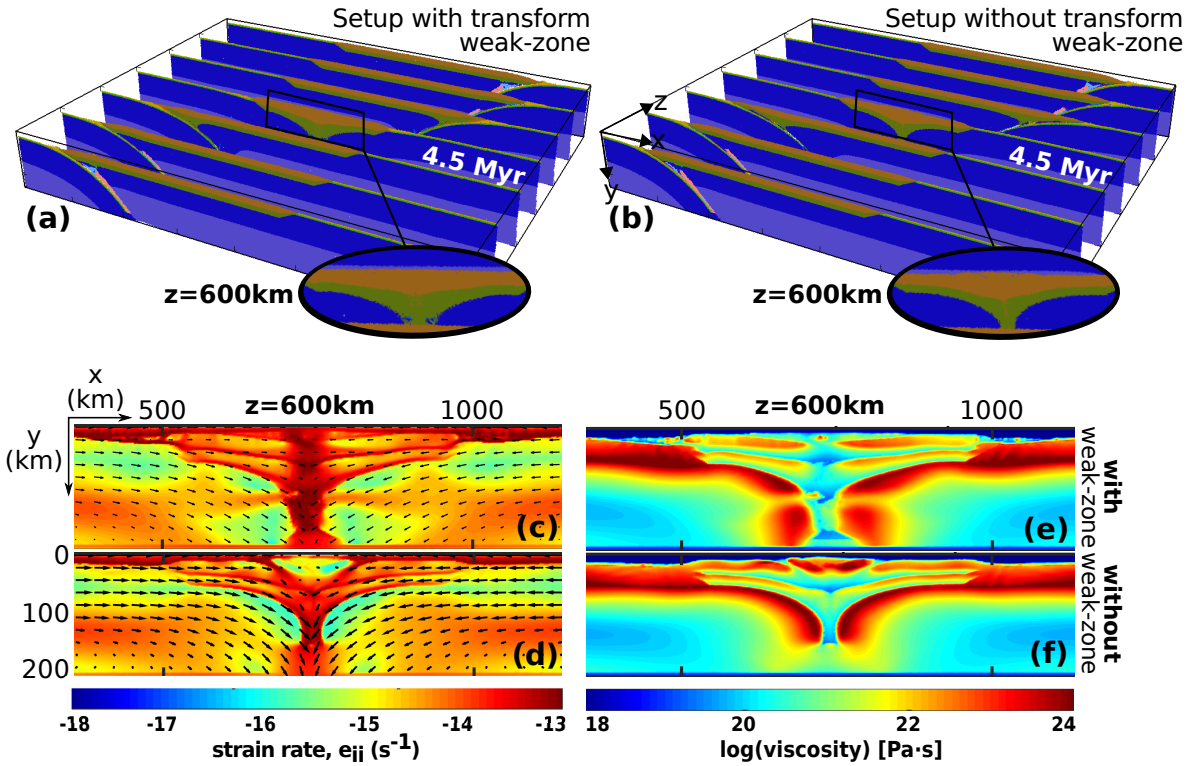

Figure 4-6: Modelling results of model setups with (a,c,and e) and without (b,d, and f) transform weak-zone which initially connects the two subduction zones. All visualisations in this Figure are from around 4.5 Myr.

4-3-3 Variation of subduction zones offset

In this set of models, the subduction lengths are kept constant at 400 km, while the subduction zones offset varies as followed: kitd–300 km; kitk–500 km; and kitl–700km. The visualisations of this set of models are shown in Appendix B. The subduction zones in all three models develop in a similar manner. Figure B-1 shows that the subduction zones in all three model develop high topography in the fore-arc regions.

Due to having the smallest subduction zones offset, the subduction zones in kitj reaches the centre of the transform by 2 Myr (Figure B-2c), which is a few million years earlier than kitk and kitl. The distinct differences are mainly in the transform section. In the case of kitj, by the time the continental crust starts to segregate (at around 1 Myr) (Figure B-5f) the subduction zones appears to be reaching the centre of the transform already.

By 2.7 Myr (Figure B-2d and B-4h), the centre of the transform in kitj resembles a convergence between the two subduction zones, since there is only 300km-wide continental crust between the two subduction zones.

At z=600 km, of viscosity and strain-rate cross-sections of kitk (Figure B-7(f-j) and B-7(f-j)) and kitl (Figure B-9(f-j) and B-9(f-j)) display similar characteristics as the reference model (kitd). Figure B-9h shows that kitl seems to be the only model in Set 3 to exhibit the faulting features (similar to those observed in the reference model) on the flanks of the transform.

Such narrow continental crust in kitj also explains why there is only a brief period (around 1 Myr) of crustal thickening and shortening, which is clearly illustrated in the composition visualisation (Figure B-2b). This short period of crustal shortening and thickening also means a short period of surface uplift, shown in Figure 4-3 (a-c). From the Figures, it can be seen that the uplift starts to build up from 1 Myr (Figure 4-3a) before the maximum topography is reached around 2 Myr (Figure 4-3b), and the topography in the central part of the transform starts to decrease and disintegrate after 3 Myr (Figure 4-3c).

4-4 Influence of one-sided collision transform

In all of the previous models, the prescribed weak-zones were set up in a symmetrical fashion. Another model, kitm (Table 3-2), was constructed in order to add some asymmetry. The model kitm also represents the one-sided collision transform setup. The subduction zones setups in kitm are similar to those in the reference model (subduction length=400 km and subduction zones offset=900 km). The key difference is that the prescribed transform weak-zones is now dipping in one direction (eastwards) only, as illustrated in Figure 4-7a.

The visualisations of evolution of rock compositions are displayed in Figure 4-7. The subduction zones evolves in a similar manner as other previous models. The viscosity cross-sections at z=375 km (Figure 4-9(a-e)) shows a region in the transition zone, where the prescribed weak-zone is under the rim of the continental crust. Around 1 Myr (Figure 4-9b), the upper and lower continental crust starts to segregate and the lower continental crust is dragged down into the mantle, as observed around 2 Myr (Figure 4-9c). The molten hydrated crustal composition appear from 2 Myr onwards (Figure 4-9(c-f)).

In Figure 4-7, the cross-sections at z=400 km and z=800 km shows the evolution of compositions in the transition zone (between the subduction zones and the transform). At the

transition zones, both the materials from the upper and lower continental crust are dragged down into the mantle by subduction. In the meantime, in the vicinity of the subduction margins, the lower continental crust appear to intrude upwards into the upper continental crust, as observed in Figure 4-7(b-f). The slab-tearing of the lower continental crust is observable at around 2 Myr (Figure 4-7c) on the cross-sections northwards and southwards of the transform.

The transform in kitm initially evolves in a similar manner to the transition zones due to the subduction weak-zone being placed right below the continental crust, as shown on a cross-section at z=600 km in Figure 4-7a. From then onwards, both layers of the continental crust are pinched down along the prescribed weak-zone, as illustrated in Figure 4-7b. The upper continental crust appear to be pinched down to the depth y≈50 km, after which its downward motion seems to terminate, while the lower continental crust continues to sink along the weak-zone (Figure 4-7c). The centre of the transform exhibits the slab-tearing, of the lower continental crust, from 4 Myr onwards (Figure 4-7e and f) which is a few million years after the slab-tearing in the transition zones.

The centre of the transform still exhibits the thickening and shortening of the continental crust, similar to the reference model (kitd). However, in the case of kitm, the crustal thickening is mainly localised on the east (right) side of the continental crust. This is observable throughout the composition cross-sections in Figure 4-7. The strain-rate cross-sections (Figure 4-8) also reinforce the one-sided crustal thickening. The strain-rate cross-sections at z=600 km (Figure 4-8(f-j)) shows layers of high strain-rate, which signifies the stress within the layers of continental crust, localising mainly in the eastern (right) side of the transform.

The cross-sections displaying kitm's viscosity evolution are shown in Figure 4-9. At the centre of the transform (z=600 km), the cross-section from 2 Myr onwards (Figure 4-9(h-j)) appear to show features of the western (left) half of the lower continental crust underthrusting under the eastern (right half). The western-half upper mantle (the lowest layer of the high-viscosity layers) at z=600 km also appear to be underthrusting beneath the eastern continental crust (Figure 4-9(i and j)).

The surface expression of kitm develops in a similar fashion to the reference model. However, in kitm, high topography along the transform appears as a single straight segment without any partition, as shown in Figure 4-10. Such a straight transform arose from the fact that the whole transform region was designed to subduct in one direction only. The high-topography regions above the subduction zones start to pull apart from the transform segment at around 3 Myr (Figure 4-10c). By 4 Myr (Figure 4-10d), the three distinctively high topographic regions appear as three separated peaks. The surface expression above the transform in kitm shows a significantly less complexity than Set 2 and 3 models where the transforms are allowed to evolved without prescribed weak-zones.

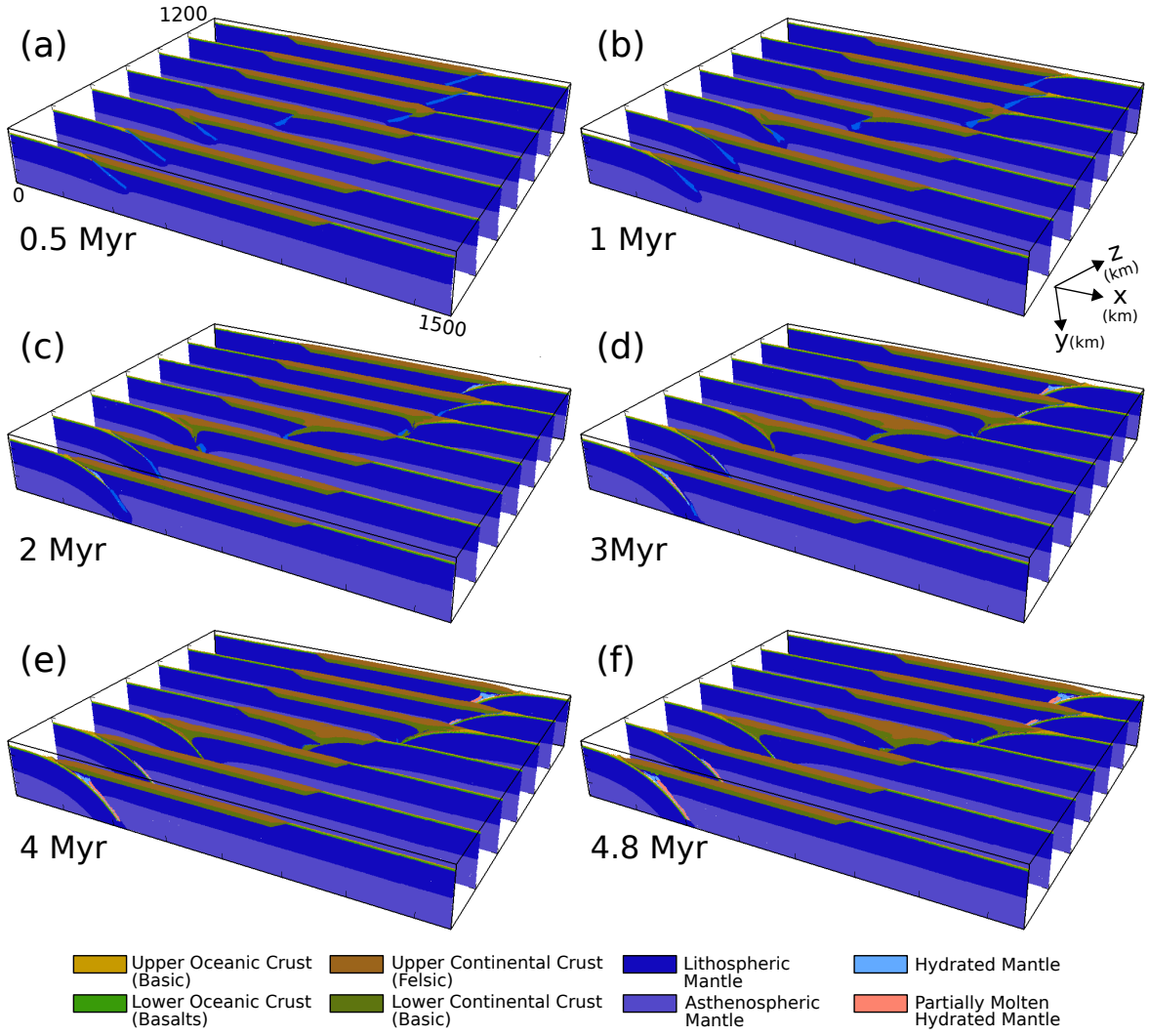

Figure 4-7: The composition evolution of a model with one-sided collision transform weak-zone (kitm).

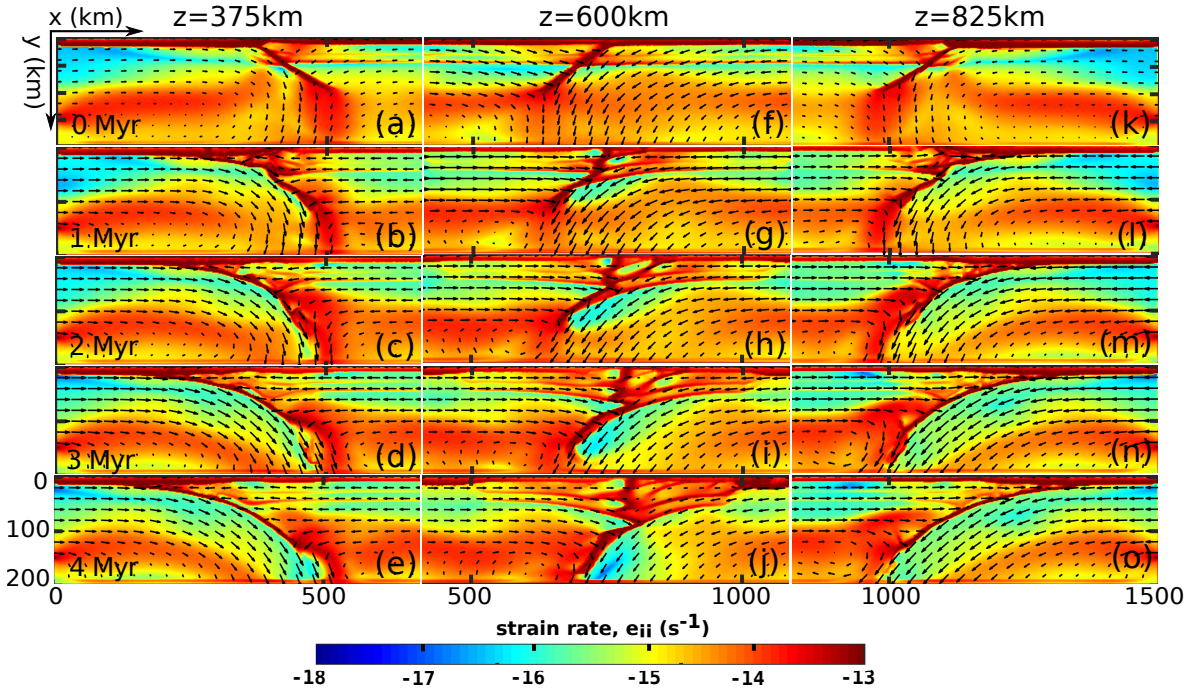

Figure 4-8: The strain-rate development of a model with one-sided collision transform weak-zone (kitm).

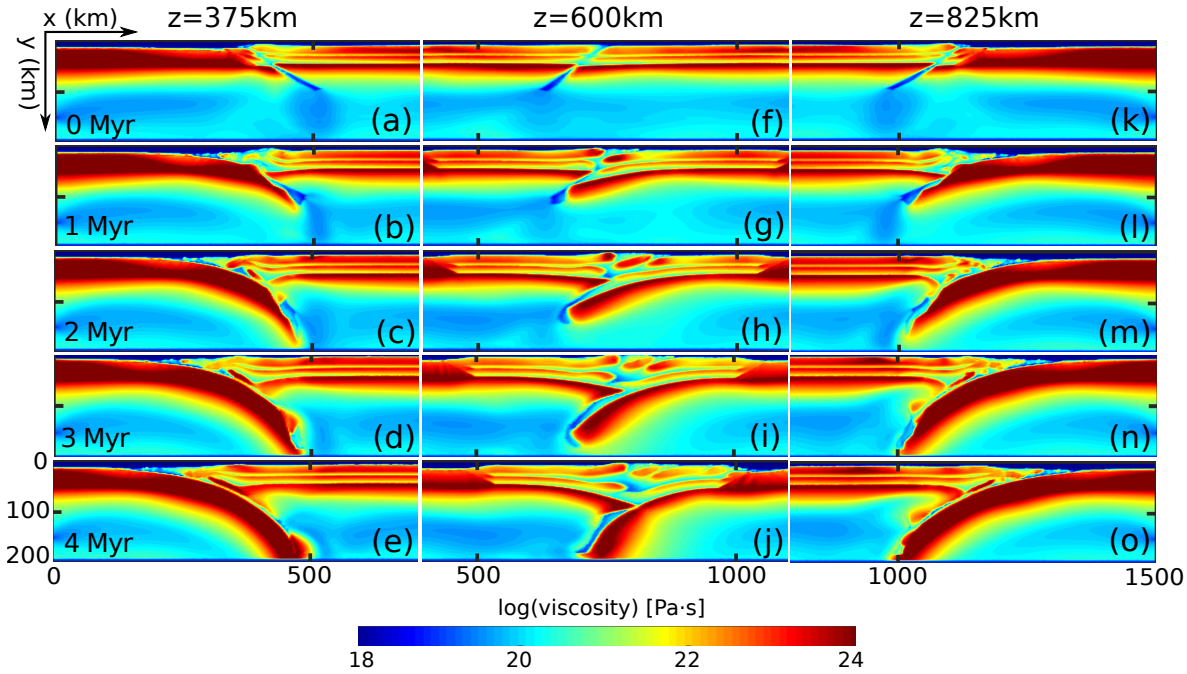

Figure 4-9: The viscosity evolution of a model with one-sided collision transform weak-zone (kitm).

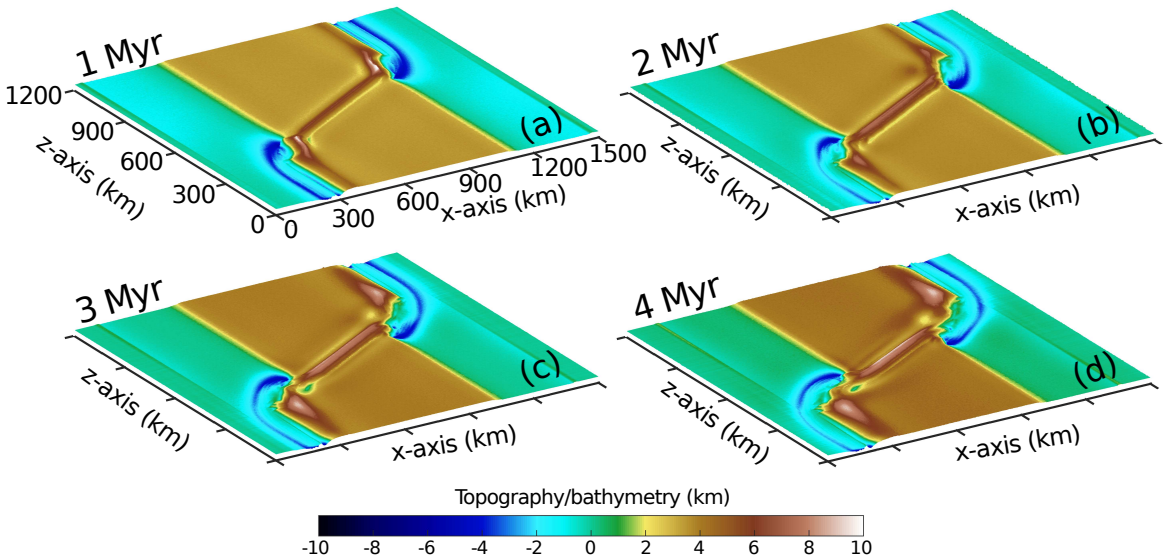

Figure 4-10: The Topographic/bathymetric evolution of a model with one-sided collision transform weak-zone (kitm).

Chapter 5

Discussion

5-1 3D Geometry

Set 1 models suggest that it is important for the initial model setup to be implemented with a continental crust feature. The presence of a continental crust plays a key role in producing the (continental) crustal thickening and shortening characteristics, which are of great importance in terms of mountain building.

This numerical modelling study also suggests that the lithospheres at the subduction zones sink down with the greatest downward velocity, $v_y \approx 53.65$ mm/year. This is evidenced in the 3D visualisation of the lithospheric structure (Figure 5-1) where the subduction zones appear to be the first regions to have reached the model boundary (y=200 km), while the transform zone follows suit. The lithospheres in the transform zone sink down obliquely (Figure 5-1c). The downward angle of the subduction zones, as well as the transform, change throughout the 10 Myrs, implying that this continental transform system does not appear to be attaining a long-term steady state, but instead evolve continuously due to the relative motions of the lithosphere.

A comparison of 3D geometry between different weak-zone setups can be drawn from the models in this study. The different weak-zones setups are: (i) Two-sided Collision (twisted) Transform (Figure 5-2a and d); (ii) One-sided Collision Transform (Figure 5-2b and e); and (iii) No Transform (Figure 5-2c and f). The significant and notable features are as followed:

- The development of the upper continental crust differs from one setup to another. In the case of two-sided collision (Figure 5-2a), the upper crust develop with little (to none) major fragmentation on both sides of the collision. This is due to the presence of a weak-zone, which force the system to release the stress downwards along a specific path, and therefore the upper crust experiences very little compression.

- The upper continental crust in the no-transform setup (Figure 5-2c) is fragmented into 3 major structures. In this setup, the two plates collide without a pre-define pathway to relieve stress, so the whole volume (from top to bottom) experiences a similar magnitude

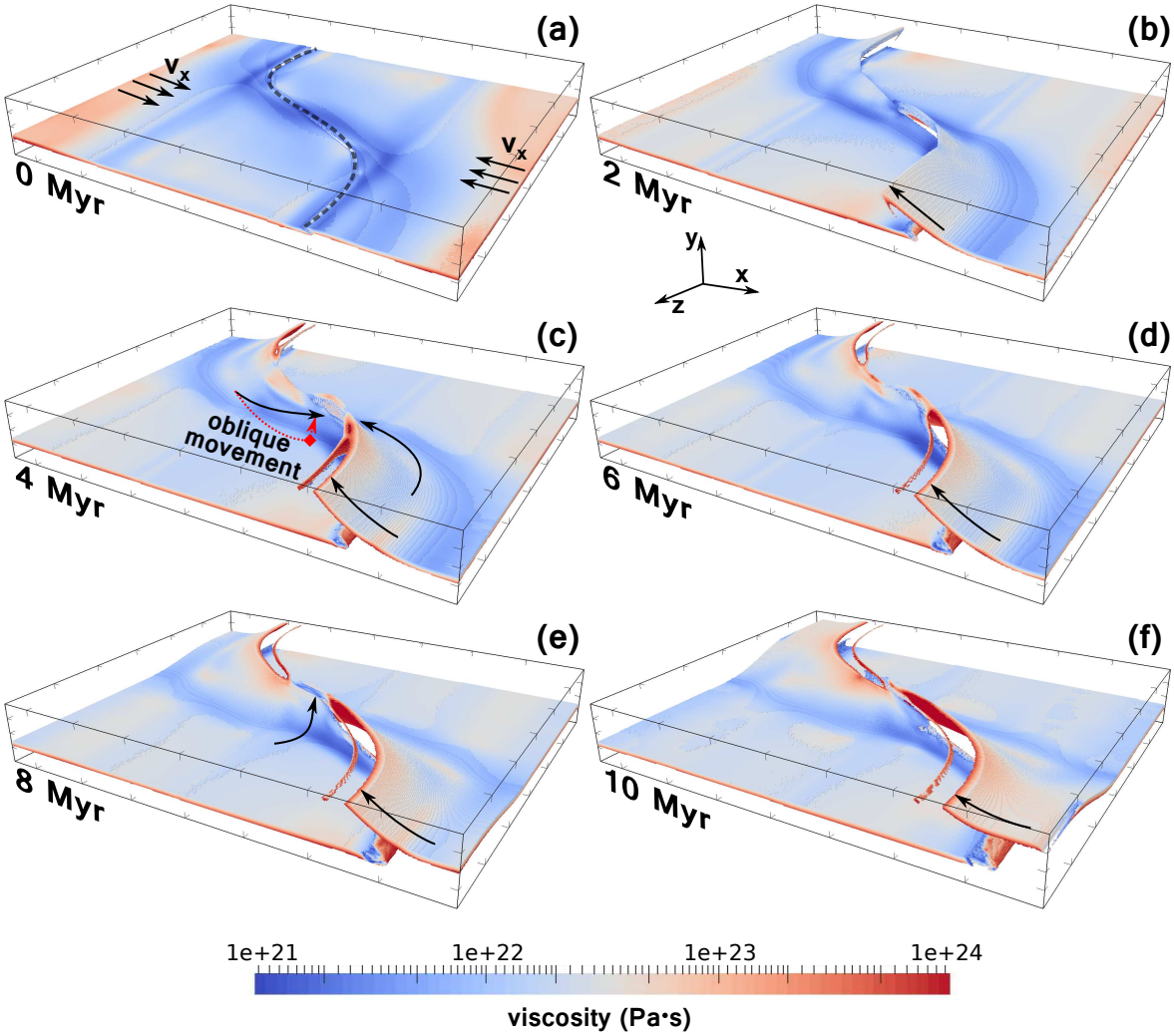

Figure 5-1: An upside-down view of 3D structural development of the reference model (*kitd*). The slab here is extracted from the temperature range 1000°C-1250°C.

of stress, hence the fragmentation of the upper crust. The middle block of upper crust appears to be underthrusted by the crusts on both sides. The lower continental crusts from both sides relieve stress by subducting downwards. The layers of high strain-rate (Figure 5-2f) signify the relative motion between the upper and the lower continental crust, which allows each crustal layer to respond to stress differently.

- In the one-sided collision setup, the fragmentation and deformation of the upper continental crust is mainly localised on the subducting plate, as outlined on Figure 5-2b. No crustal fragmentation is observed on the left slab. The lower crust on the right side underthrusts the lower crust on the left slab. The lithospheric mantle of the left slab appears to be pushing against the subduction (right) slab; this movement pinches out the lower crust material in the process, which then leads to slab-tearing.

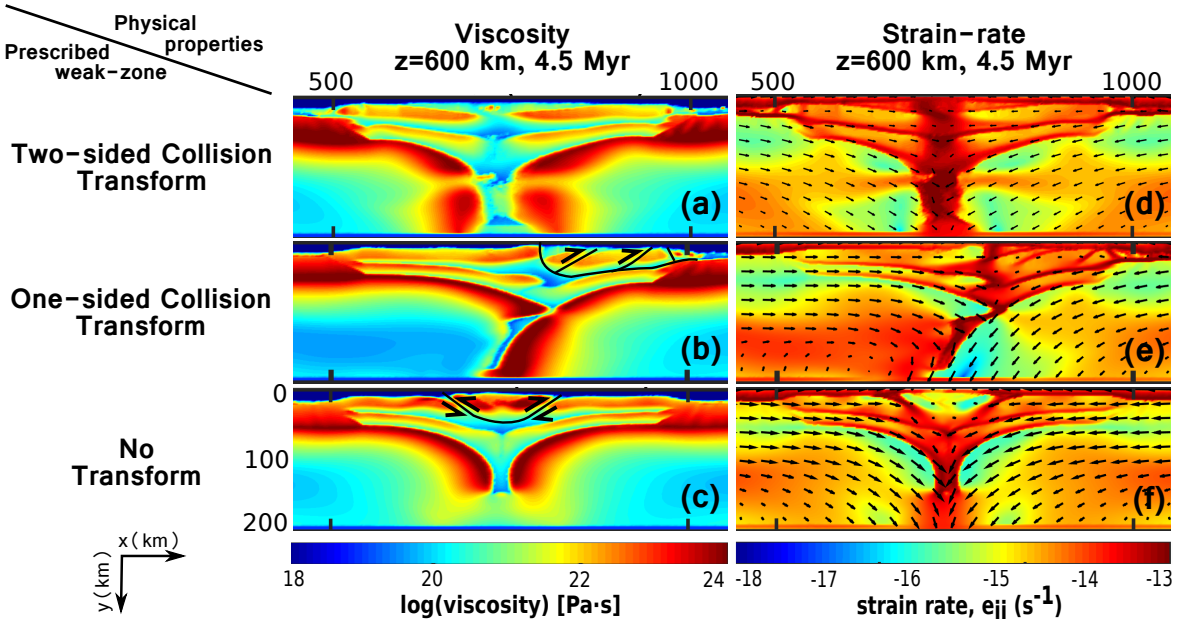

Figure 5-2: Comparing the cross-section (z=600 km) of the transform zone in different weak-zone setups: (i) Two-sided Collision (twisted) Transform (Figure 5-2a and d); (ii) One-sided Collision Transform (Figure 5-2b and e); and (iii) No Transform (Figure 5-2c and f).

5-2 Topographic Development

The topographic development observed in this investigation vary among different setups. The topographic and bathymetric development in the subduction zones, however, appear to be consistent throughout their evolution. The regions with the highest topography is localised along the edge of the continental crust. These high-topography regions next to the subduction zones shares a few common characteristics:

- Firstly, the highest topography on the continental crust (along the subduction margins) are localised around the points connecting the subduction segments to the transform segment. A plausible explanation for such observation could be that the regions close to the transform segment might experience greater degree of obliquity than in the straight subduction zone. Also, these 'joining' points accommodate both the stress caused by the migration of subduction (towards the transform) and the stress from the models' intrinsic relative plate motion which is constantly pushing the continental crust against the subducting plate. The accumulated stress from several directions causes a large uplift of the upper continental crust, hence the regions of distinctively high elevation.

- The second common feature is the width of these high-topography regions. An observation at the time around 4.8 Myr, shows that all of the models (of different setups) attain such high-topography regions with a common width of 80-100 km. The no-transform setup produced the peaks with the highest topography, $\leq$10 km.

In contrast to the subduction sections, the topographic development in the transform section varies greatly among different model setups. The visualisations of the topographic development from different model setups are shown in Figure 5-3.

The models with a prescribed 'twisted' weak-zone, Figure 5-3a and b, in the transform zone produce surface expressions of simple and predictable geometry. The topography of these models develop as straight segments which lie on either side of the transform, depending on the dipping direction of the weak-zones. The high-topography segments lie on the sides with greater tendency to sink down along the weak-zone first. These segments of high topography, each lies on the opposite side of the transform, eventually merges into one segment as the system evolves.

The model with prescribed weak-zone dipping only in one direction, Figure 5-3c and d, produces topographic features of even simpler geometry than those discussed previously. Despite producing interesting internal structural features, the surface expression from this model setup is a single straight segment of high topography, initially extending from one subduction zone to another. The topographic development from this model setup gives a clear illustration of the shortening of the transform. By 4.8 Myr (Figure 5-3d) , the length of this high-topography segment has decreased by 54% from its initial length, observed at 1 Myr.

In contrast to the other two setup, the no-transform setup produces a, generally, more complex topographic features. Prior to 2 Myr (Figure A-1e), the topographic development from this setup surprisingly show similar trend to the setups with prescribed weak-zones in the transform region; a long straight segment of high topography is observed. At around 2 Myr, as the transform is getting more compressed by the subduction zones on both ends, the uplifted and initially-straight segment starts to exhibit a structural trend (on the surface) which resembles a sinusoidal wave, as shown in Figure 5-3e. This surface expression reflects how the model 'naturally' accommodates the stress imposed on a segment which extends the width of the continental crust. By 4.8 Myr, Figure 5-3f, the topographic features are noticeably more complex than in the other two setups. The attained peaks over the transform has the highest elevation ($\leq$10 km) compared to the peaks in similar regions produced by other model setups. The characteristics of these uplifted peaks over the transform resemble a mountain range, to some extent, especially the presence of multiple peaks, as well as the valleys between them. Similar to the other two model setups, the topographic visualisation from this setup also exhibit the shortening of the transform segment. The overall plane of the transform (on the surface) also appears to be rotating towards the a plane parallel to the x-axis.

One specific feature which I was hoping to observe through the topographic development of these model setups is the 'islands gap', which is a channel (low topography) sitting in-between New Zealand's North Island and South Island, an example is circled in Figure 5-3d. This spot of contrastingly low topography is situated between the region representing the North Island (upper subduction zone) and the region representing the South Island (the transform). This feature, at the specific location, shows up sparsely throughout the topographic evolution of every models. However, this feature does not seem to persist through the development, and even disappear all together in most models.

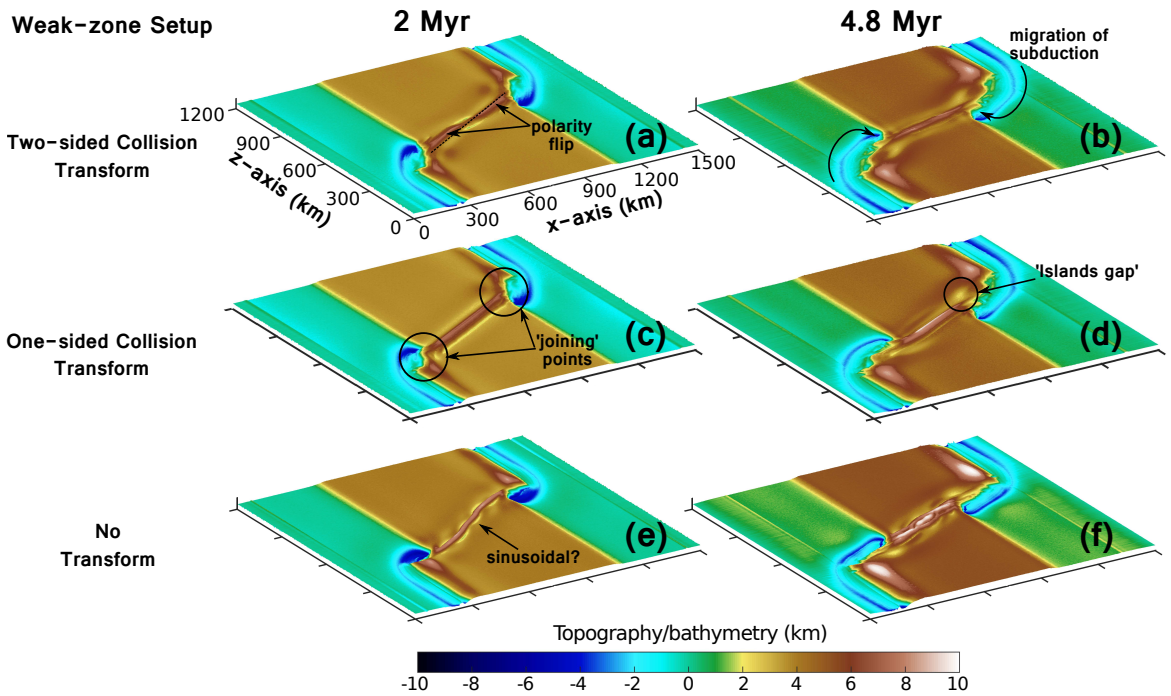

Figure 5-3: Comparing topographic development between setups with different prescribed weak-zone geometry.

5-3 Fault/Stress Development

This investigation uses strain-rate visualisations to gain an insight into faulting activity that occur throughout the model evolutions. A first-order comparison is drawn between models of different weak-zone setups: (i) Two-sided Collision Transform (Figure 5-4(a-e)); (ii) One-sided Collision Transform (Figure 5-4(f-j)); and (iii) No Transform (Figure 5-4(k-o)).

In the two-sided collision model setup, the strain-rate evolution of the subduction zones stays at the highest value (-12 s^{-1}), as an intact strand, throughout the model evolution. In general, there are not a lot of major faulting activity in the subduction zones. As the subduction zones migrate towards the transform, some faults develop and extend to the transform. The regions surrounding the transform exhibit a lot of faulting activities. Some splay fault systems develop at both ends of the transform segment, as shown in the circled region in Figure 5-4d.

The strain-rate development produced by the one-sided collision setup exhibits similar characteristics as the results produced by the two-sided collision setup. The splay faults at both ends of the transform also develops in this setup (Figure 5-4i).

The no-transform setup produces features which are different from the other two setups. Around 1 Myr (Figure 5-4k), high strain-rate is localised as a straight segment over the transform, which connects the two subduction zones. By 2 Myr (Figure 5-4i), the segment of high strain-rate starts to take shape after a sinusoidal wave, which is similar to the topographic observation on the surface. From 4 Myr onwards (Figure 5-4n and o), the main transform strand appears to be splitting and develops into branches of faults, opposing to the other two setups (Figure 5-4e and j) where the main transform strand appears to persist throughout the evolution.

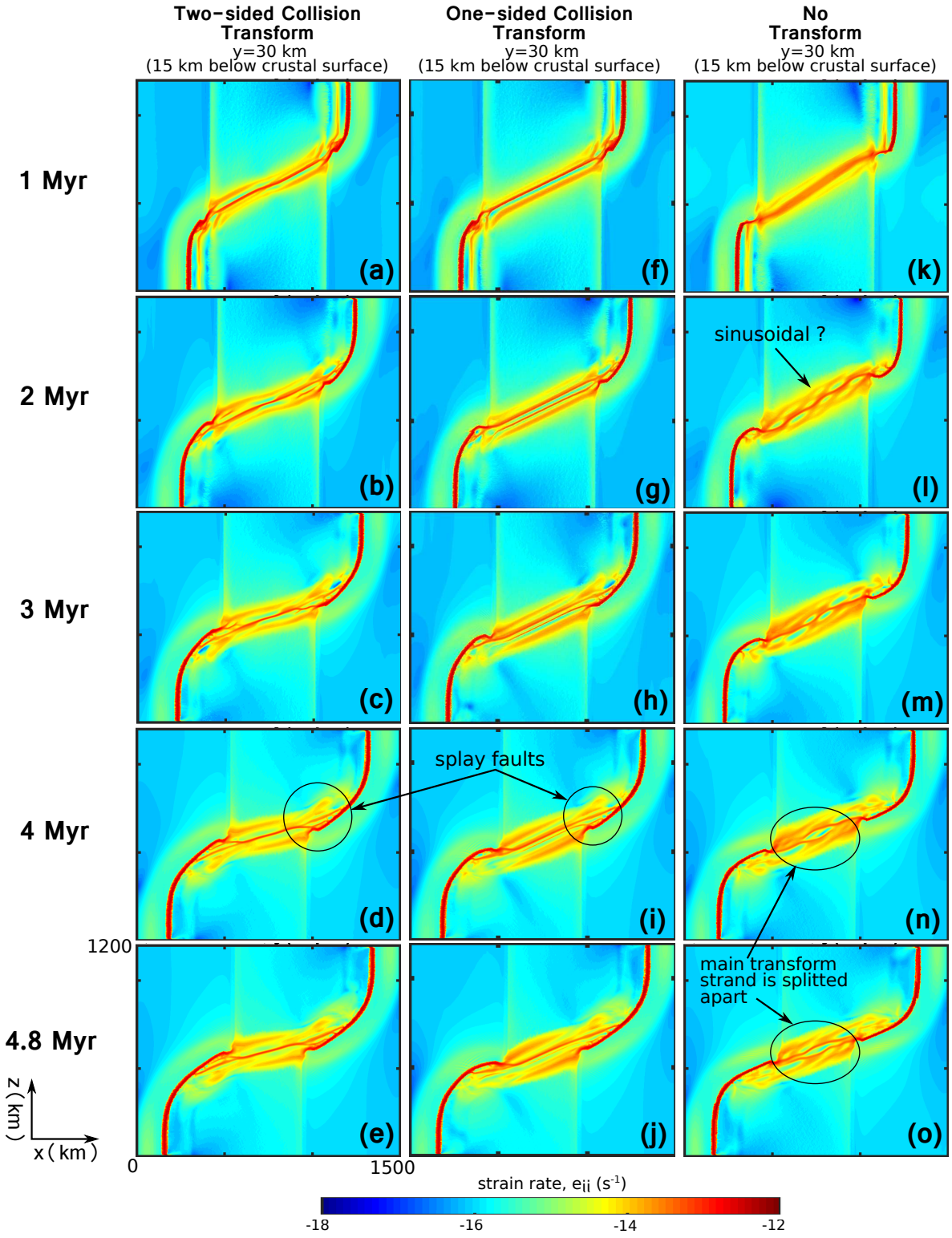

Figure 5-4: Comparing faults/stress development (using strain-rate visualisation) between setups with different prescribed weak-zone geometry: two-sided collision transform (a-e); one-sided collision transform (f-j); and no-transform setup (k-o).

5-4 Comparison with natural observations

5-4-1 Central Alpine Fault

Preliminary comparison is made with results from this investigation (one-sided collision model setup) and the interpretation of SIGHT transects (Norris and Toy, 2014; Lamb et al., 2015). The South Island Geophysical Transect (SIGHT) project imaged a major continental transform fault to lower crust-upper mantle depths with seismic methods (Stern et al., 2007).

Figure 5-5 displays the viscosity cross-sections, resulted form this numerical studies, and the interpretation from natural features observed through the SIGHT transects. The location of the two SIGHT survey lines are shown in FIgure 2-1. The natural observations from the literatures (Figure 5-5c and d) are viewed from a plane perpendicular to the Alpine Fault. The viscosity cross-sections, Figure 5-5a and b, are viewed from, both, perpendicularly and obliquely to the transform.

The modelling results, from both viewpoints, exhibit steep-angle Alpine Fault. The Alpine Fault viewed perpendicular (Figure 5-5a) to the transform is interpreted to be almost vertical, and less so when viewed obliquely to the transform (Figure 5-5b). This specific feature can be compared to the upper continental crust observed in nature. Both interpretations from the literatures also exhibit steeply-dipping Alpine Fault in the upper 20-30 km.

The modelling results show that the upper crust of the Australian Plate is pushed against the Alpine Fault and thrusts upwards. This contradicts the SIGHT transects' interpretations, since the Pacific side is observed to be thrusting upwards, hence the Southern Alps.

Both of the viscosity cross-sections also show faulting blocks in the upper continental crust (upper 20-30 km). This feature is better illustrated in the oblique view, where one can see the large faulting blocks, in the upper crust, spreading eastwards (Pacific side). These faulting blocks are consistent with the interpretation of SIGHT-1 transect (Figure 5-5d) where three major fault planes are observed in the same region. Although, these faulting blocks are not explicitly interpreted by Lamb et al. (2015) (Figure 5-5c), the localisation of earthquake occurrences (high seismic activity) reflects that there appear to be faulting planes in the same region as the modelling results (Figure 5-5a) and SIGHT-1 interpretation (Figure 5-5d).

Another comparable feature is the thickening of the lower continental crust. As illustrated in the oblique cross-section, Figure 5-5a, the lower crust is thicken at x=750-900 km, with the thickest region localising right beneath the Alpine Fault. The structures of the modelling results suggest that this thickened lower crust could have arisen from the overlapping of the lower crusts from both the Australian and the Pacific Plates. This feature also show up in the interpretation of, both, SIGHT-1 and SIGHT-2 transects.

5-4-2 Marlborough Fault System

Figure 5-6 displays the preliminary comparison between the strain-rate at the depth 15 km below the surface (Figure 5-6a and b) and the surface expression observed in nature, specifically in the Marlborough Fault System (MFS) (Figure 5-6c). The strain-rate slices (xz-plane) are from two weak-zone setups, Two-sided and One-sided Collision Transform.

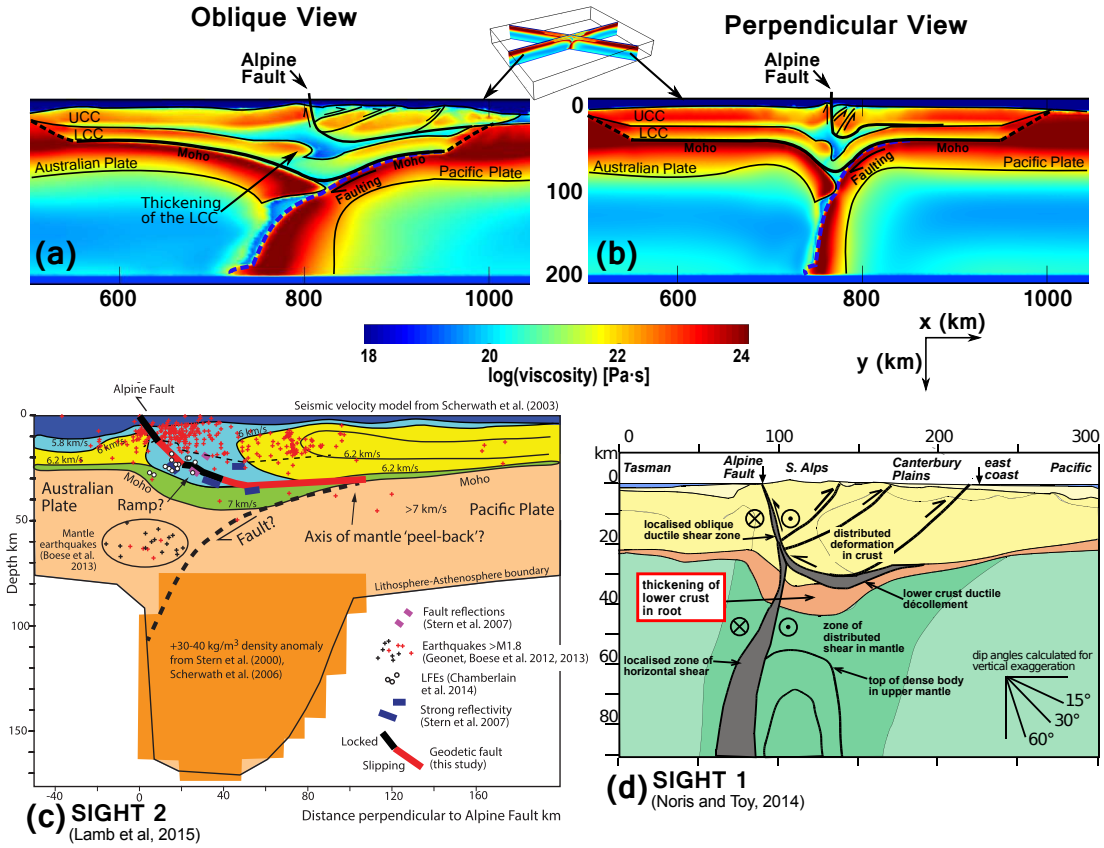

Figure 5-5: A comparison between the interpreted modelling results and natural observations, at central Alpine Fault. The interpretation of modelling results are shown in 2 view points: (i) Oblique (a) and (ii) Perpendicular (b) to the transform. The nature observations comprise the interpretation of SIGHT-2 transect by Lamb et al. (2015) (c) and the interpretation of SIGHT-1 transect by Norris and Toy (2014). Three aspects are comparable: (i) Characteristic of Alpine Fault; (ii) Thrusting faults on the upper continental crust; and (iii) The thickened lower continental crust. UCC and LCC are abbreviated for Upper- and Lower-Continental Crust, respectively.

The strain-rate slices are interpreted in terms of faulting structures. The development from both model setups display similar general characteristics. The two-sided collision setup appears to have developed three major faults with a small fault connected to the northernmost strand, all of which branched out from the the straight Alpine Fault. The one-sided collision setup developed four major faults, all of which branched out from the Alpine Fault. The fault development from the two model setup, in general, reflect striking resemblance to the fault patterns observed in nature.

One point which contradicts with the natural observation is the continuation of the Alpine Fault into the MFS. In nature, the Wairau Fault (northernmost) is a direct continuation of the Alpine Fault, however, in the model results, it appears that the northernmost faults stem from the Alpine Fault, rather than continue on from it.

Another interesting aspect is the age progression of the activation of each fault in the MFS. In the MFS, the ages of activation of each strike-slip fault become increasingly younger towards

the south-east direction (King, 2000; Furlong, 2007; Wannamaker et al., 2009; Norris and Toy, 2014). This trend of fault-activation is exhibited in the modelling results. Although the northernmost faults (W*) in the models are not direct continuation of the Alpine Fault, they showed up as soon as 0.2 Myr after the simulation was initiated and have persisted through the evolution. The rest of the faults, then, started to branch out from the Alpine Fault.

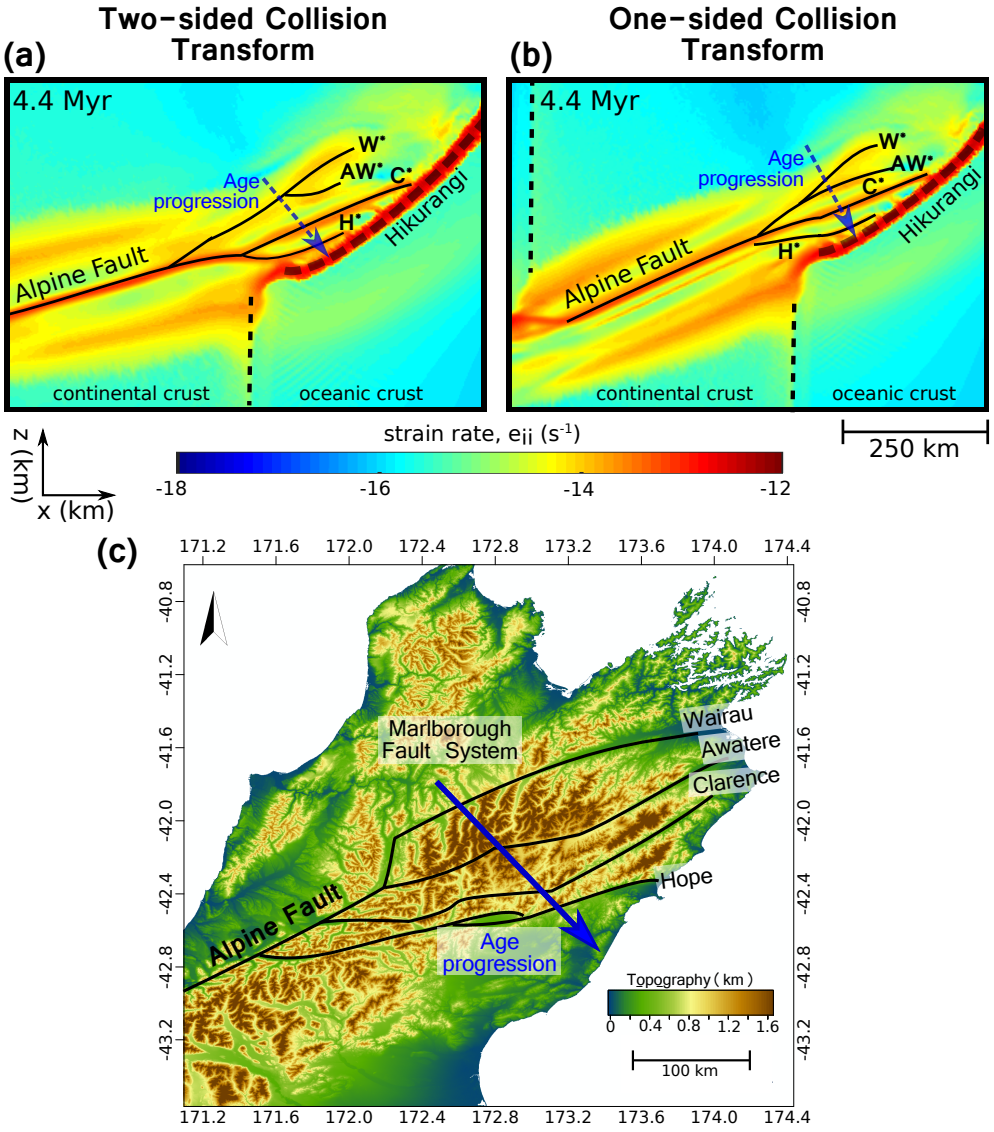

Figure 5-6: Comparison of first-order features observed between the interpreted faults from modelling results ((a) two-sided and (b) one-sided collision transform) and the fault patterns observed in the Marlborough Fault System (MSF) (c). The strain-rate visualisations at the depth of 15 km into the crust are used to reflect the faulting patterns and fault planes. Two aspects of interests are (i) The development of splay faults and (ii) The ages of initiation of faults in the MFS. The asterisked letters in (a) and (b) denotes which interpreted fault has the potential to become which MFS fault. [Topographic data used to plot (c) is obtained from Jarvis A., H.I. Reuter, A. Nelson (2008)]

5-5 Model Assumption and Limitation

The geometry of the prescribed weak-zones in all of the model setups were deliberately simple. This allowed us to isolate whichever parameter to investigate, and allowed us to study the first-order features of the tectonic evolution of subduction zones and continental transform system. In nature, these lithospheric weak-zones bound to be more structurally complex and unstructured, therefore further investigation is required.

5-6 Research Prospect

None of the models in this investigation produced topographic features which are comparable to natural observations. A suggestion for an improvement on the model setup lies in the geometry of the continental crust. Instead of having a single big slab of continental crust implemented in the model, one can implement the continental crust as observed in the present-day setting of New Zealand. The top (northern) half of the continental crust could be shifted to the west (Challenger Plateau), while the bottom (southern) half is shifted to the east (Campbell Plateau). This setup could, similarly, be tested with and without the prescribed transform weak-zones, although a one-sided collision transform set up is encouraged since it produced promising structural features in the subsurface.

Chapter 6

Conclusions

A state-of-the-art 3D thermomechanical modelling is used to gain insights into the tectonic evolution and the structural styles of New Zealand. Several model setups were constructed to simulate the evolution of a system, which comprises two subduction zones, Hikurangi (north) and Puysegur (south), and a continental transform, the Alpine Fault. The finite-differences code ('I3ELVIS') iteratively solves the conservation laws in a staggered grid. The study comprises three types of model setups, with an intention to evaluate the controls, which the geometry of the prescribed weak-zones have, on the tectonic evolution. The key weak-zones setups are: (i) Two-sided Collision Transform; (ii) One-sided Collision Transform; and (iii) No Transform. The No-Transform model setups also comprises of different models investigating the influence of different geometry of the subduction zones.

From the numerical investigation, the conclusions are the following:

1. **Steady state** – The continental transform system does not appear to be attaining a steady state, but instead continues to develop throughout the simulation.

2. **Common features** – All of the model setups exhibit some similar general features, all of which are consistent with natural observations, as well as previous studies. The key features are (i) an oblique continental transform and (ii) the migration of the subduction zones towards the transform.

3. **Topographic features** – The model setups with two-sided and one-sided collision transform, both, developed simple topographic features with several similarities when compared to each other. In contrast, the no-transform model produced a more complex and nature-like surface expressions, which indicate a potential for further modification and investigation.

4. **Structural development** – The one-sided collision model setup produced a transform with the most promising 3D structural features, which are: (i) the steeply dipping Alpine Fault; (ii) the thickening of the lower continental crust in the continental collision zone; and (iii) the presence of the thrusting fault-blocks in the upper continental crust.

5. **Faults development** – The two-sided and one-sided collision model setups clearly illustrated the splaying of faults at the end of the transform. The first-order observation of these splay faults appear to be comparable to the faults in Marlborough Fault System.

Bibliography

Braun, J. and Beaumont, C. (1995). Three-dimensional numerical experiments of strain partitioning at oblique plate boundaries: implications for contrasting tectonic styles in the southern Coast Ranges, California, and central South Island, New Zealand. *Journal of Geophysical Research*, 100(B9):18,18–59,74.

DeMets, C., Gordon, R. G., and Argus, D. F. (2010). Geologically current plate motions. *Geophysical Journal International*, 181(1):1–80.

Furlong, K. P. (2007). Locating the deep extent of the plate boundary along the Alpine Fault zone, New Zealand: Implications for patterns of exhumation in the Southern Alps. In *Special Paper 434: Exhumation Associated with Continental Strike-Slip Fault Systems*, volume 434, pages 1–14. Geological Society of America.

Gerya, T. and Yuen, D. (2003). Characteristics-based marker-in-cell method with conservative finite-differences schemes for modeling geological flows with strongly variable transport properties. *Physics of the Earth and Planetary Interiors*, 140(4):293–318.

Gerya, T. and Yuen, D. (2007). Robust characteristics method for modelling multiphase visco-elasto-plastic thermo-mechanical problems. *Physics of the Earth and Planetary Interiors*, 163(1-4):83–105.

Harlow, F. H. and Welch, J. E. (1965). Numerical Calculation of Time-Dependent Viscous Incompressible Flow of Fluid with Free Surface. *Physics of Fluids*, 8(12):2182.

Jarvis A., H.I. Reuter, A. Nelson, E. G. (2008). Hole-filled seamless SRTM data V4, International Centre for Tropical Agriculture (CIAT).

King, P. R. (2000). Tectonic reconstructions of New Zealand: 40 Ma to the Present. *New Zealand Journal of Geology & Geophysics*, 434(43):611–638.

Lamarche, G. and Lebrun, J.-F. (2000). Transition from strike-slip faulting to oblique subduction: active tectonics at the Puysegur Margin, South New Zealand. *Tectonophysics*, 316(1-2):67–89.

Lamb, S. (2011). Cenozoic tectonic evolution of the New Zealand plate-boundary zone: A paleomagnetic perspective. *Tectonophysics*, 509(3-4):135–164.

Lamb, S., Smith, E., Stern, T., and Warren-Smith, E. (2015). Continent-scale strike-slip on a low-angle fault beneath New Zealand's Southern Alps: Implications for crustal thickening in oblique collision zones. *Geochemistry, Geophysics, Geosystems*, 16(9):3076–3096.

Le Pourhiet, L., Huet, B., and Traoré, N. (2014). Links between long-term and short-term rheology of the lithosphere: Insights from strike-slip fault modelling. *Tectonophysics*, 631:146–159.

Lebrun, J.-F., Lamarche, G., and Collot, J.-Y. (2003). Subduction initiation at a strike-slip plate boundary: The Cenozoic Pacific-Australian plate boundary, south of New Zealand. *Journal of Geophysical Research: Solid Earth*, 108(B9).

Lebrun, J.-F., Lamarche, G., Collot, J.-Y., and Delteil, J. (2000). Abrupt strike-slip fault to subduction transition: The Alpine Fault-Puysegur Trench connection, New Zealand. *Tectonics*, 19(4):688–706.

Leitner, B., Eberhart-Phillips, D., Anderson, H., and Nabelek, J. L. (2001). A focused look at the Alpine fault, New Zealand: Seismicity, focal mechanisms, and stress observations. *Journal of Geophysical Research: Solid Earth*, 106(B2):2193–2220.

McKee, S., Tomé, M., Ferreira, V., Cuminato, J., Castelo, A., Sousa, F., and Mangiavacchi, N. (2008). The MAC method. *Computers & Fluids*, 37(8):907–930.

Norris, R. J. (2004). Strain localisation within ductile shear zones beneath active faults: The Alpine Fault contrasted with the adjacent Otago fault system, New Zealand. *Earth, Planets and Space*, 56(12):1095–1101.

Norris, R. J. and Toy, V. G. (2014). Continental transforms: A view from the Alpine Fault. *Journal of Structural Geology*, 64:3–31.

Platt, J. P., Kaus, B., and Becker, T. W. (2008). The mechanics of continental transforms: An alternative approach with applications to the San Andreas system and the tectonics of California. *Earth and Planetary Science Letters*, 274(3-4):380–391.

Ranalli, G. (1995). *Rheology of the Earth*. Chapman & Hall London ; New York, 2nd ed. edition.

Reyners, M., Robinson, R., Pancha, A., and McGinty, P. (2002). Stresses and strains in a twisted subduction zone-Fiordland, New Zealand. *Geophysical Journal International*, 148(3):637–648.

Savage, M. K., Tommasi, A., Ellis, S., and Chery, J. (2013). Modeling Strain and Anisotropy Along the Alpine Fault, South Island, New Zealand. *A Continental Plate Boundary: Tectonics at South Island, New Zealand*, pages 289–305.

Scholz, C. H. (1977). Transform fault systems of California and New Zealand: similarities in their tectonic and seismic styles. *Journal of the Geological Society (London)*, 133:215–229.

Stern, T., Okaya, D., Kleffmann, S., Scherwath, M., Henrys, S., and Davey, F. (2007). Geophysical exploration and dynamics of the Alpine Fault Zone. In *A Continental Plate Boundary: Tectonics at South Island, New Zealand Geophysical Monograph Series 175*, pages 207–233. American Geophysical Union.

Sutherland, R., Davey, F., and Beavan, J. (2000). Plate boundary deformation in South Island, New Zealand, is related to inherited lithospheric structure. *Earth and Planetary Science Letters*, 177(3-4):141–151.

Walcott, R. I. (1998). Modes of oblique compression: Late Cenozoic tectonics of the south island of New Zealand. *Reviews of Geophysics*, 36(1):1–26.

Wannamaker, P. E., Caldwell, T. G., Jiracek, G. R., Maris, V., Hill, G. J., Ogawa, Y., Bibby, H. M., Bennie, S. L., and Heise, W. (2009). Fluid and deformation regime of an advancing subduction system at Marlborough, New Zealand. *Nature*, 460(7256):733–736.

Wilson, J. T. (1965). A New Class of Faults and their Bearing on Continental Drift. *Nature*, 207(4995):343–347.

Yabe, S., Ide, S., and Yoshioka, S. (2014). Along-strike variations in temperature and tectonic tremor activity along the Hikurangi subduction zone, New Zealand. *Earth, Planets and Space*, 66(1):142.

Appendix A

Set 2 Models Visualisations

A-1 Topographic/bathymetric evolution of Set 2 Models

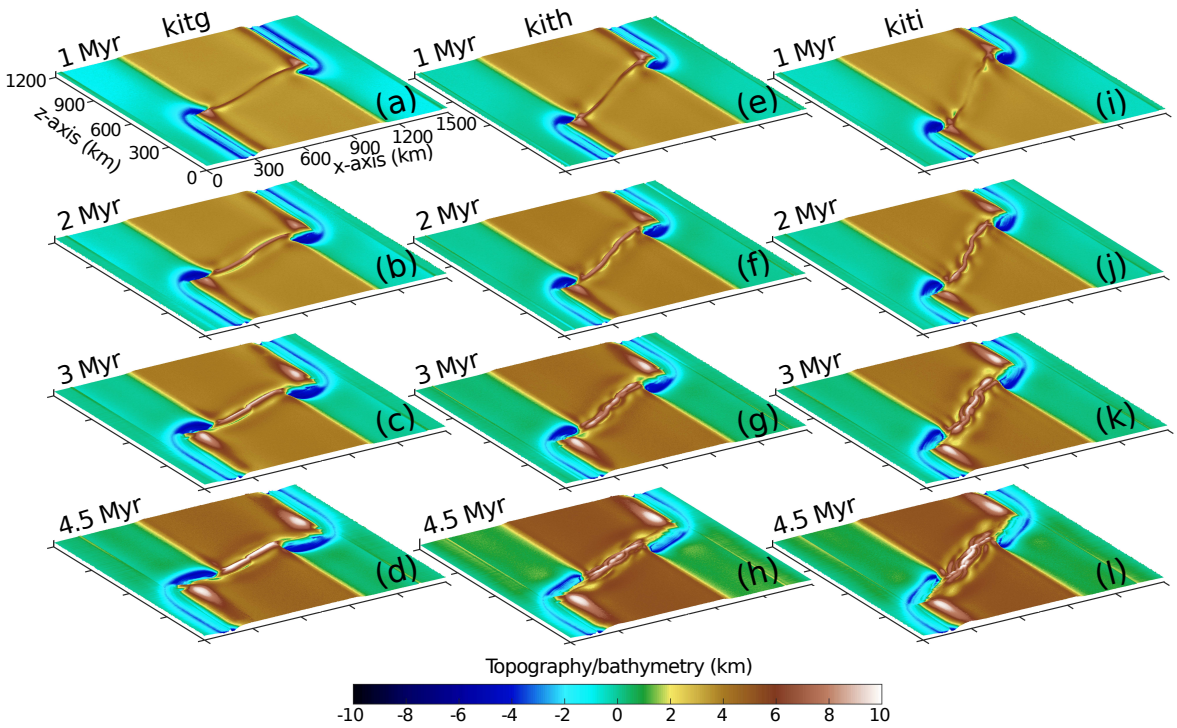

Figure A-1: Topographic/bathymetric evolution of Set 2 Models. Model *kitg* (a-d) has subduction zones of length = 500 km, *kith* (e-h) = 400 km, and *kiti* (i-l) = 300 km.

A-2 Composition evolution (3D) of Set 2 Models

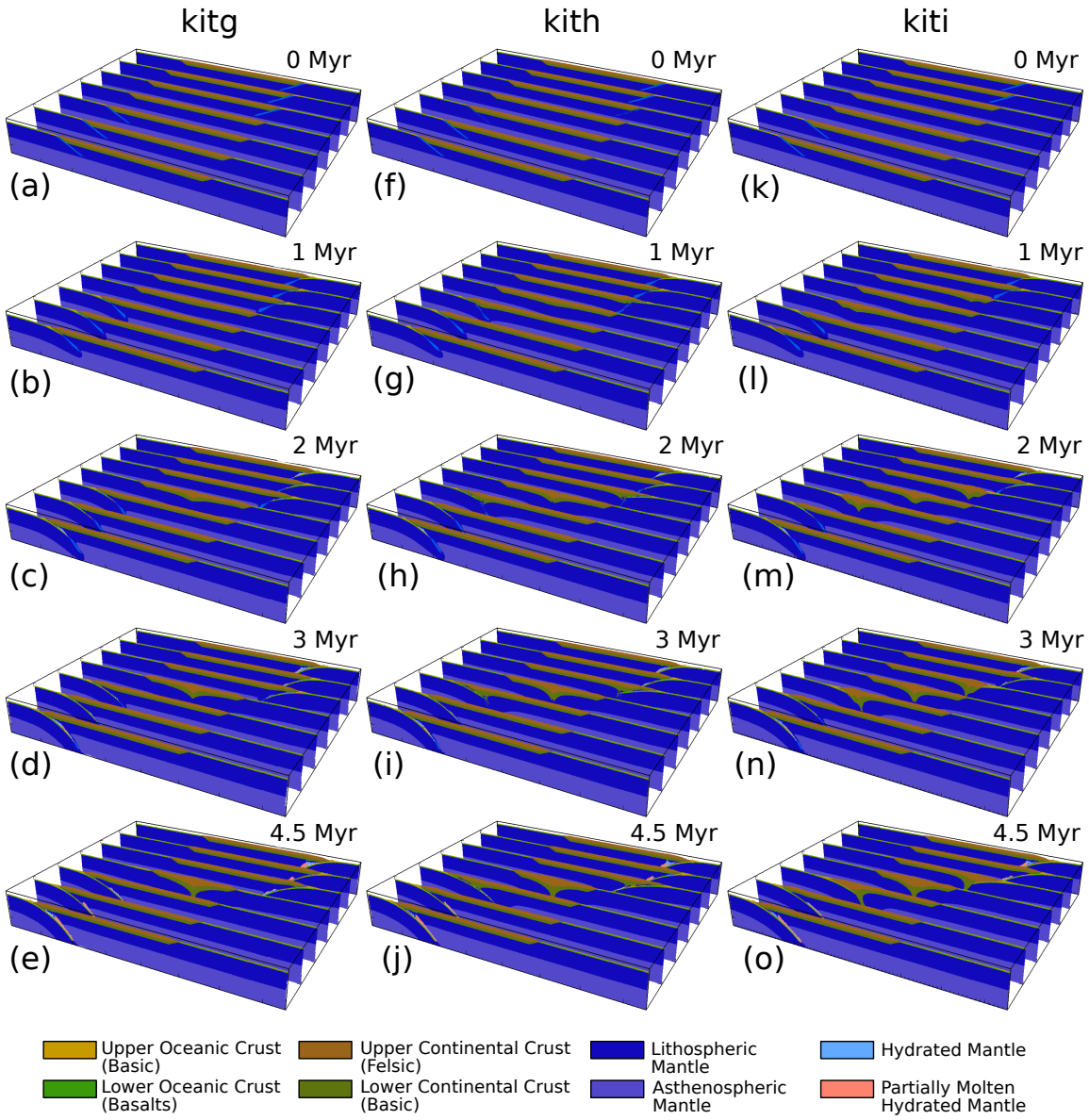

Figure A-2: The composition evolution of Set 2 Models. Model *kitg* (a-e) has subduction zones of length = 500 km, *kith* (f-j) = 400 km, and *kiti* (k-o) = 300 km.

A-3 Viscosity evolution (3D) of Set 2 Models

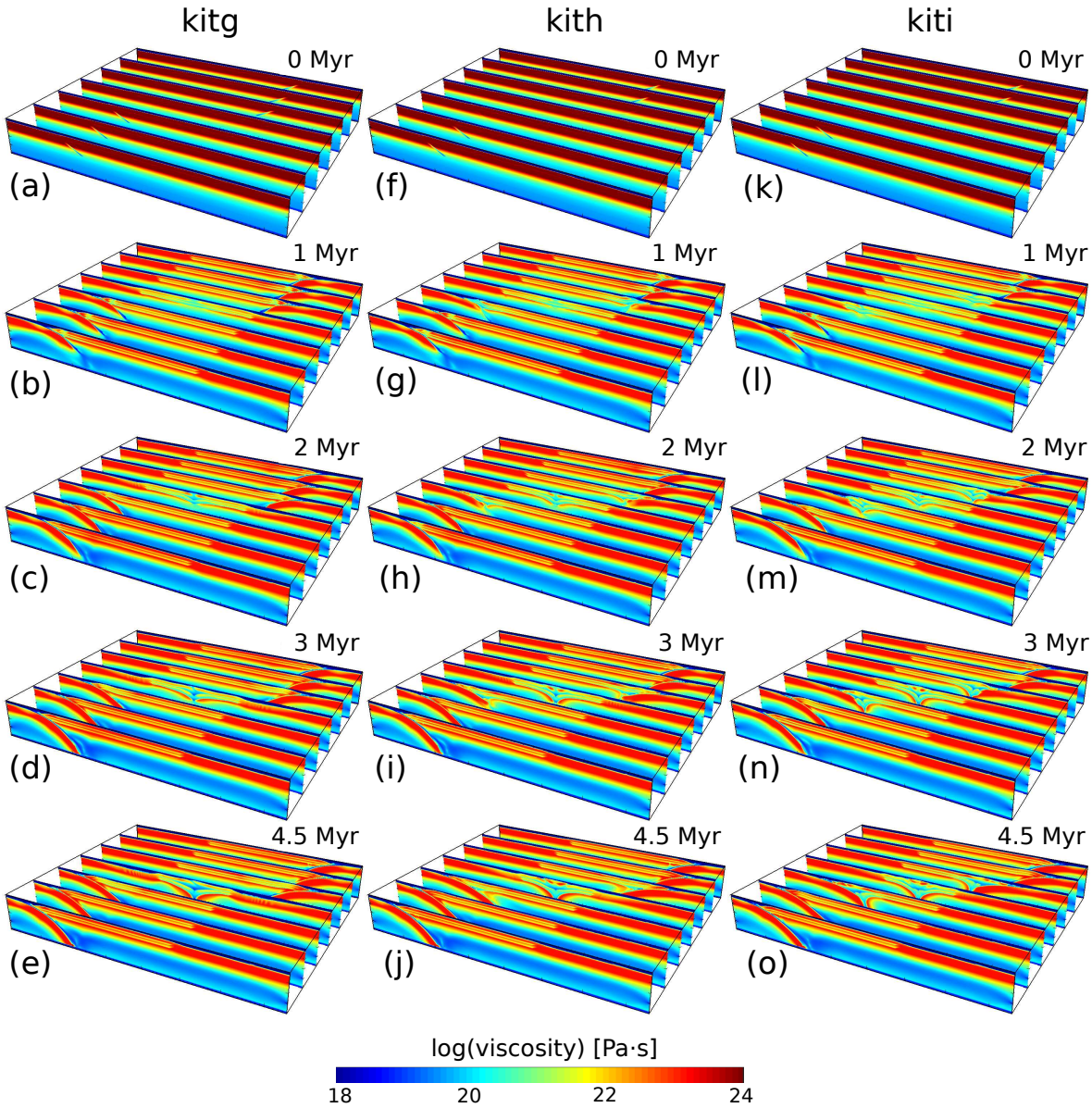

Figure A-3: The viscosity evolution of Set 2 Models. Model *kitg* (a-e) has subduction zones of length = 500 km, *kith* (f-j) = 400 km, and *kiti* (k-o) = 300 km.

A-4 kitg visualisations

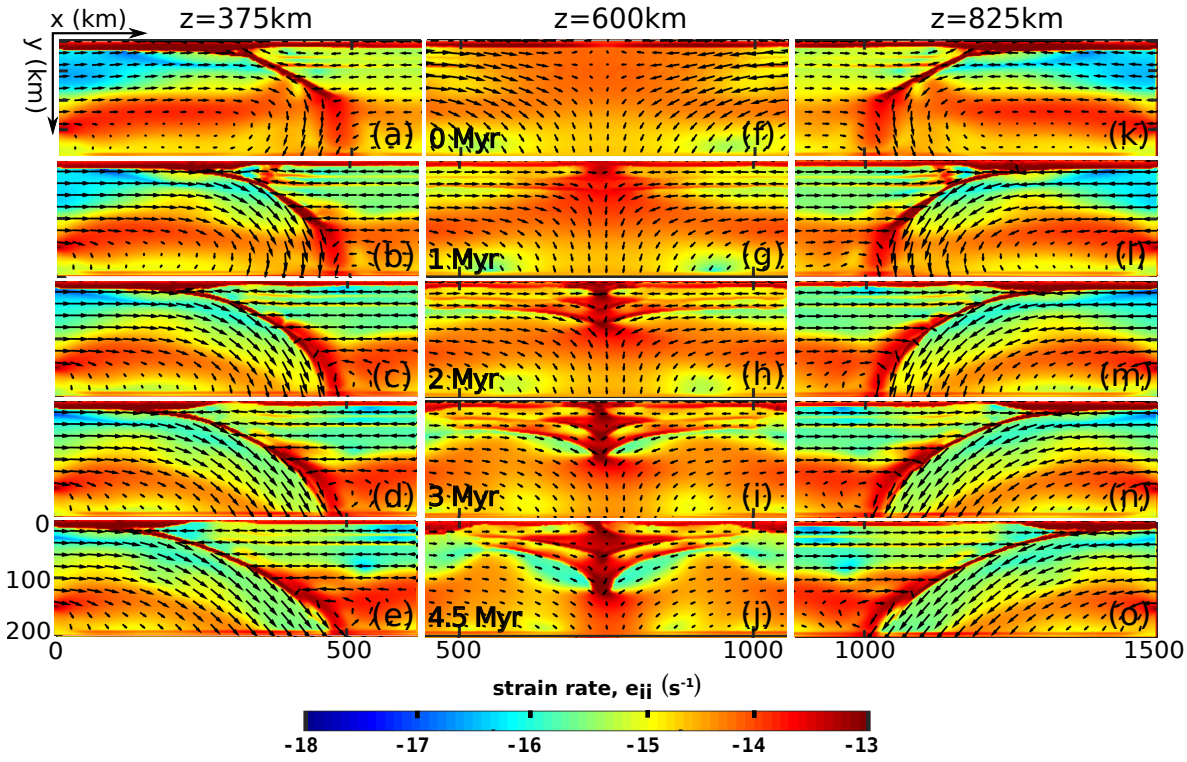

Figure A-4: Strain-rate of model *kitg*

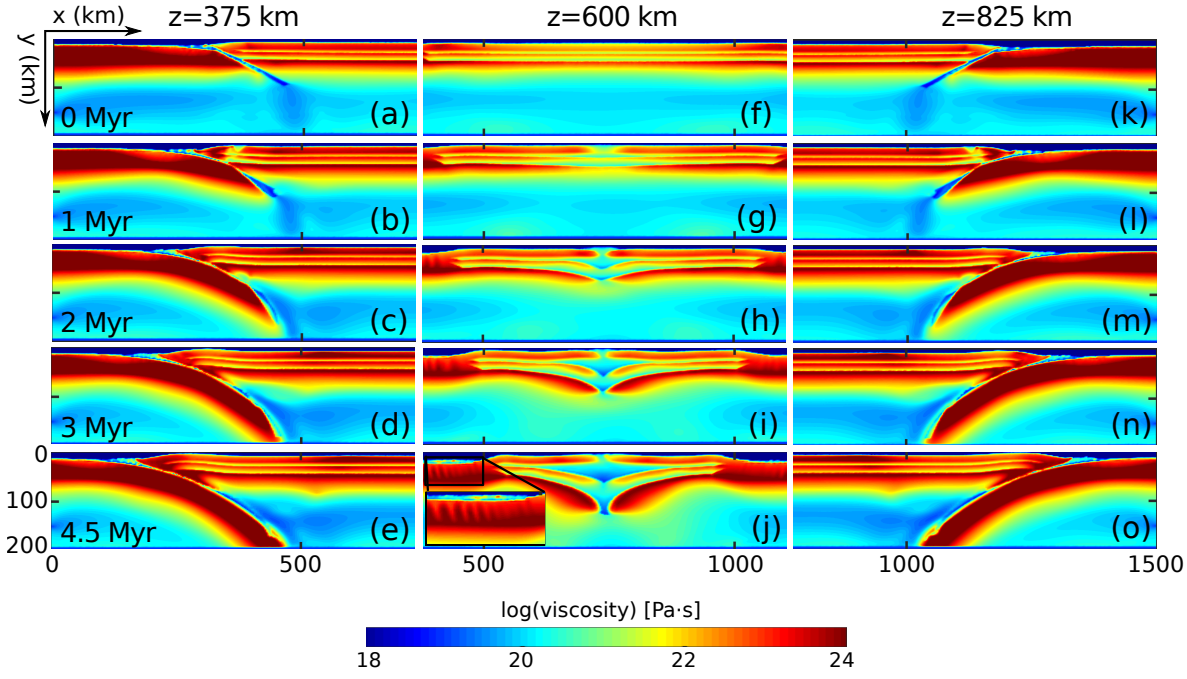

Figure A-5: Viscosity of model *kitg*

A-5 kith visualisations

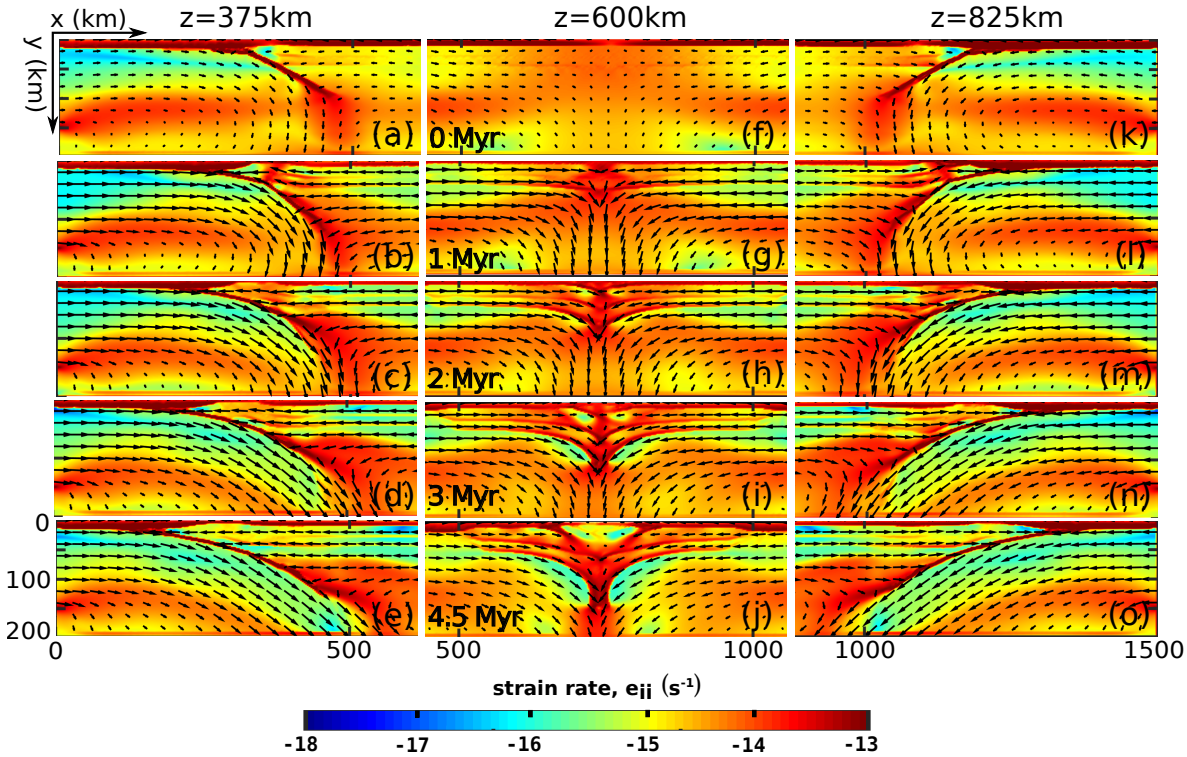

Figure A-6: Strain-rate of model *kith*

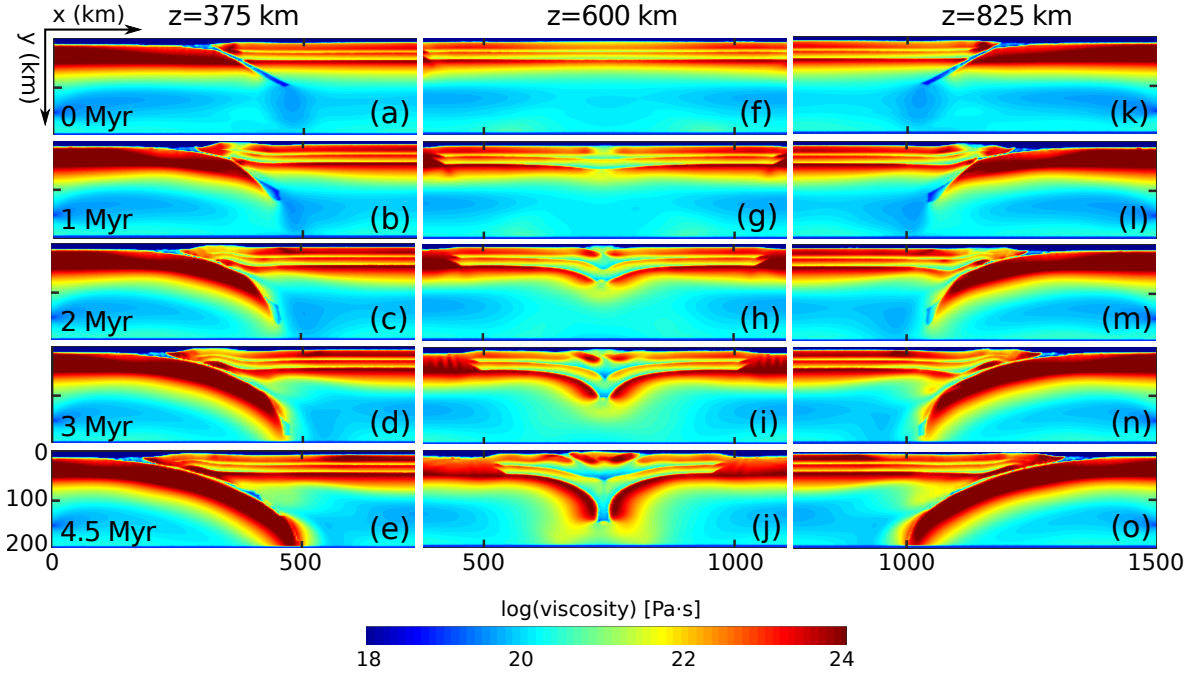

Figure A-7: Viscosity of model *kith*

A-6 kiti visualisations

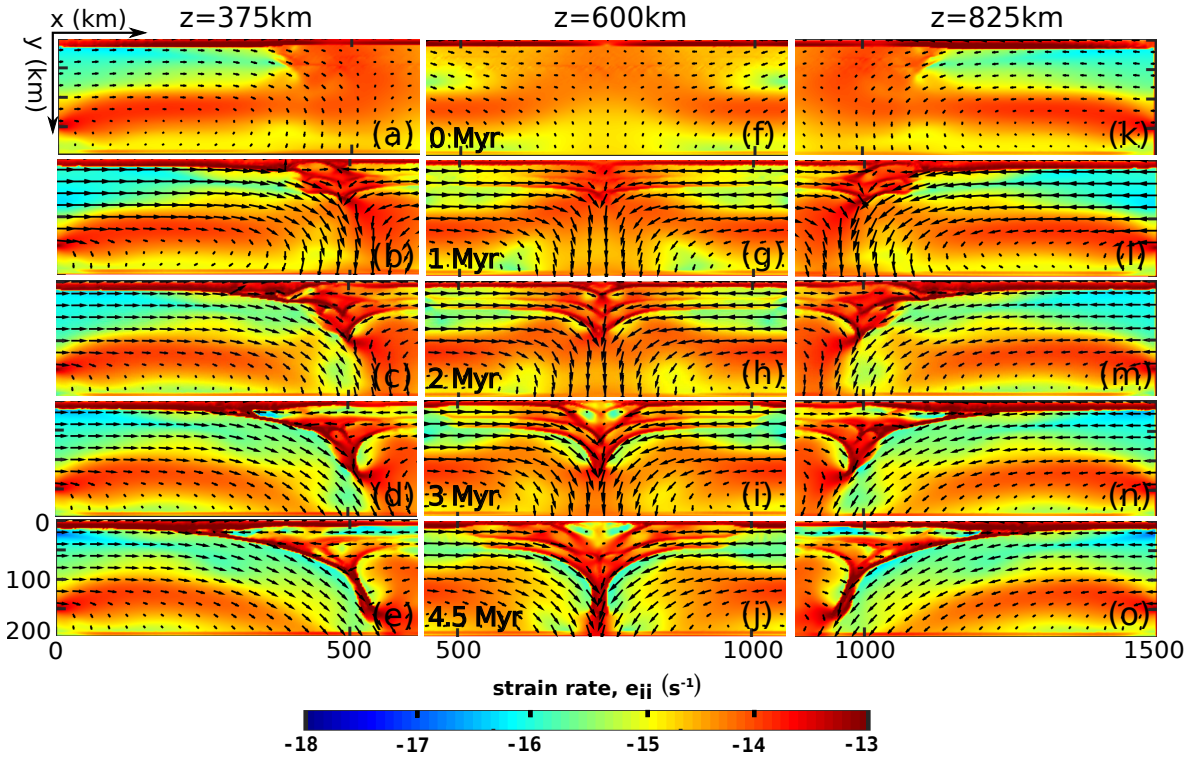

Figure A-8: Strain-rate of model *kiti*

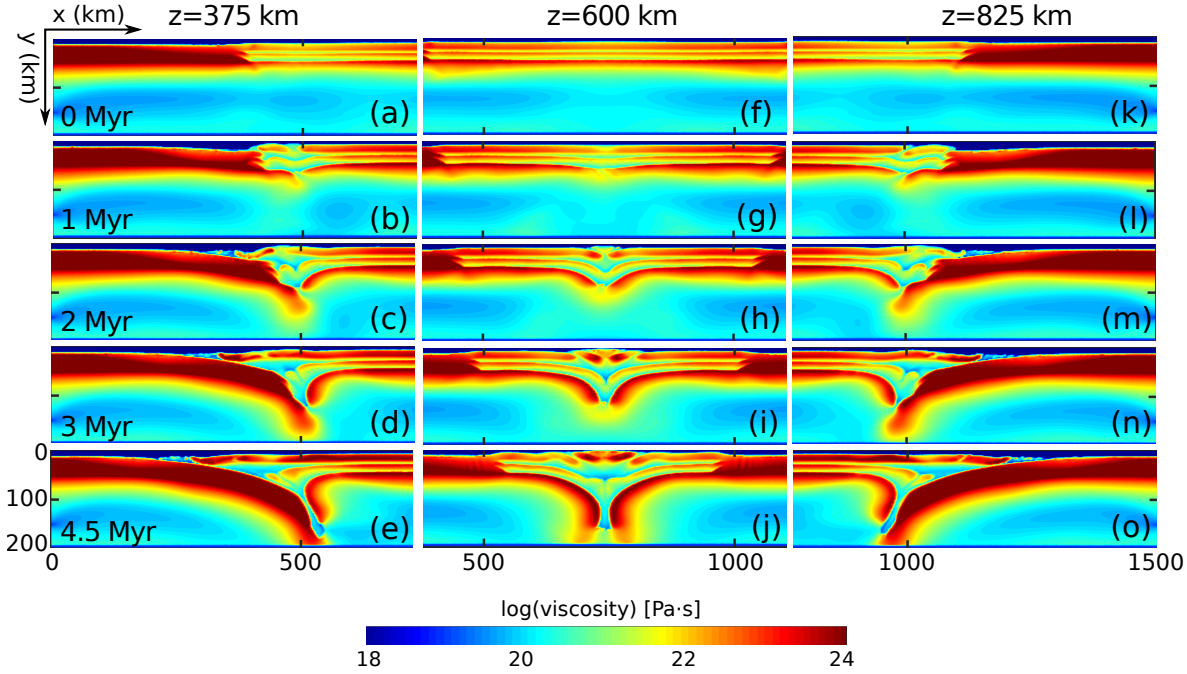

Figure A-9: Viscosity of model *kiti*

Appendix B

Set 3 Models Visualisations

B-1 Topographic/bathymetric evolution of Set 3 Models

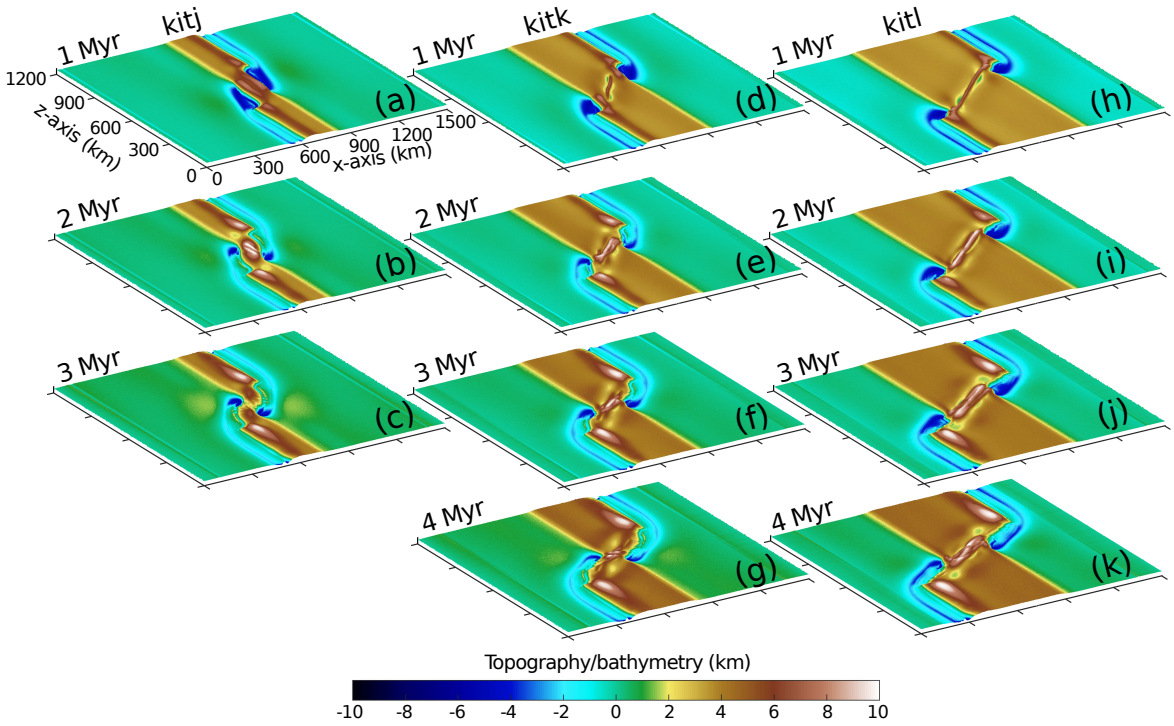

Figure B-1: Topographic/bathymetric evolution of Set 3 Models. Model *kitj* (a-c) has subduction zones separation (x-axis) = 300 km, *kitk* (d-g) = 500 km, and *kitl* (h-k) = 700 km.

B-2 Composition evolution (3D) of Set 3 Models

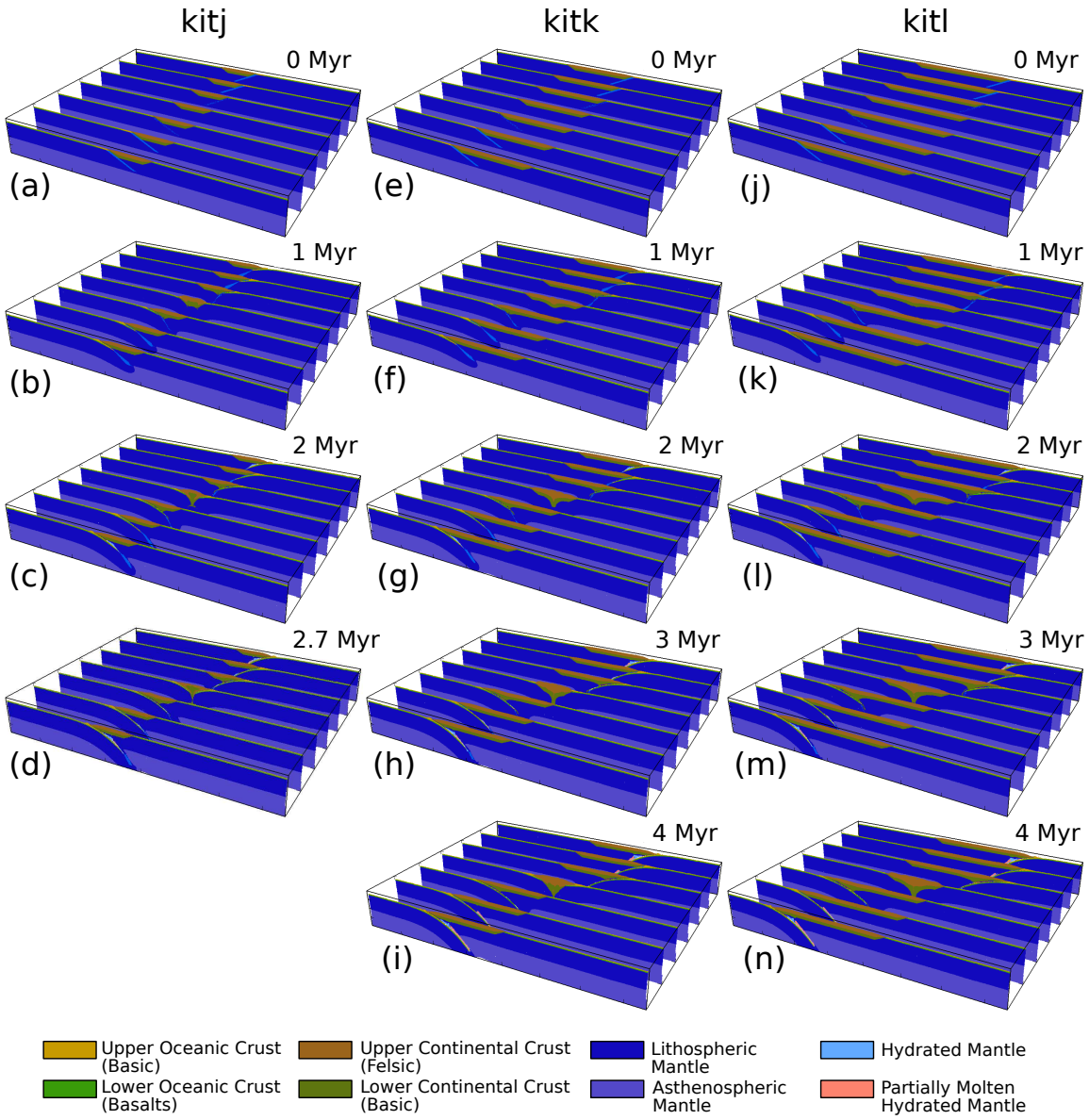

Figure B-2: The composition evolution of Set 3 Models. Model *kitj* (a-d) has subduction zones separation (x-axis) = 300 km, *kitk* (e-i) = 500 km, and *kitl* (j-n) = 700 km.

B-3 Viscosity evolution (3D) of Set 3 Models

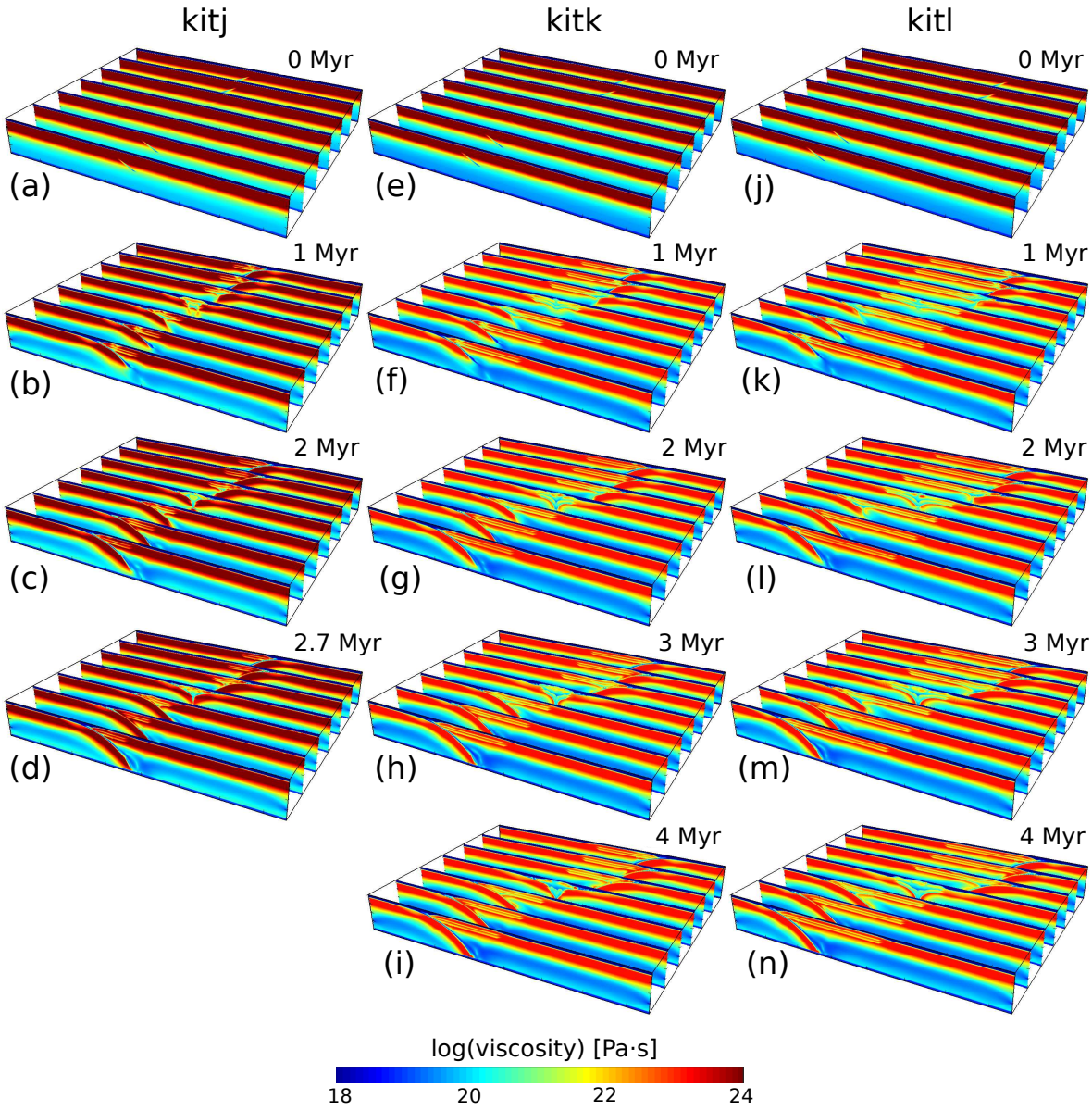

Figure B-3: The viscosity evolution of Set 3 Models. Model *kitj* (a-d) has subduction zones separation (x-axis) = 300 km, *kitk* (e-i) = 500 km, and *kitl* (j-n) = 700 km.

B-4 kitj visualisations

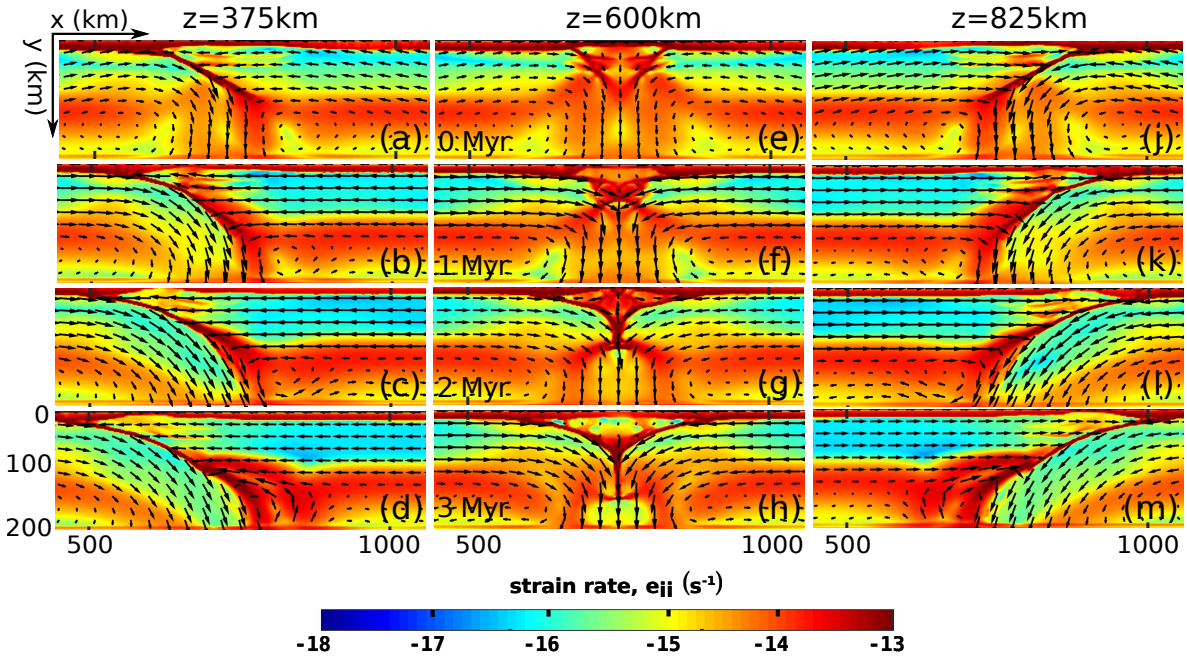

Figure B-4: Strain-rate of model *kitj*

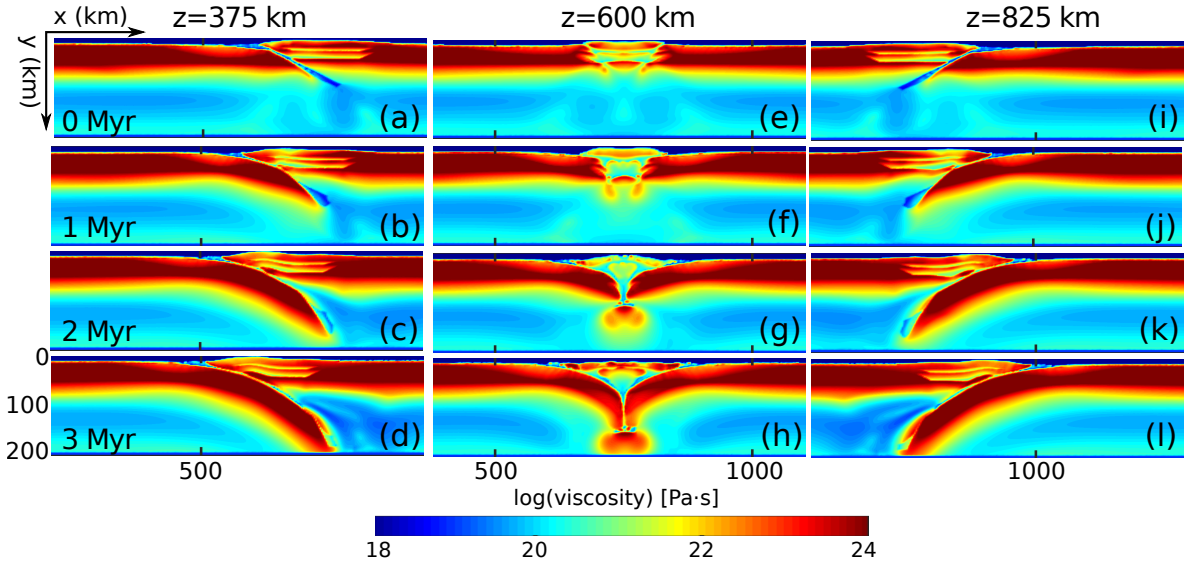

Figure B-5: Viscosity of model *kitj*

B-5 kitk visualisations

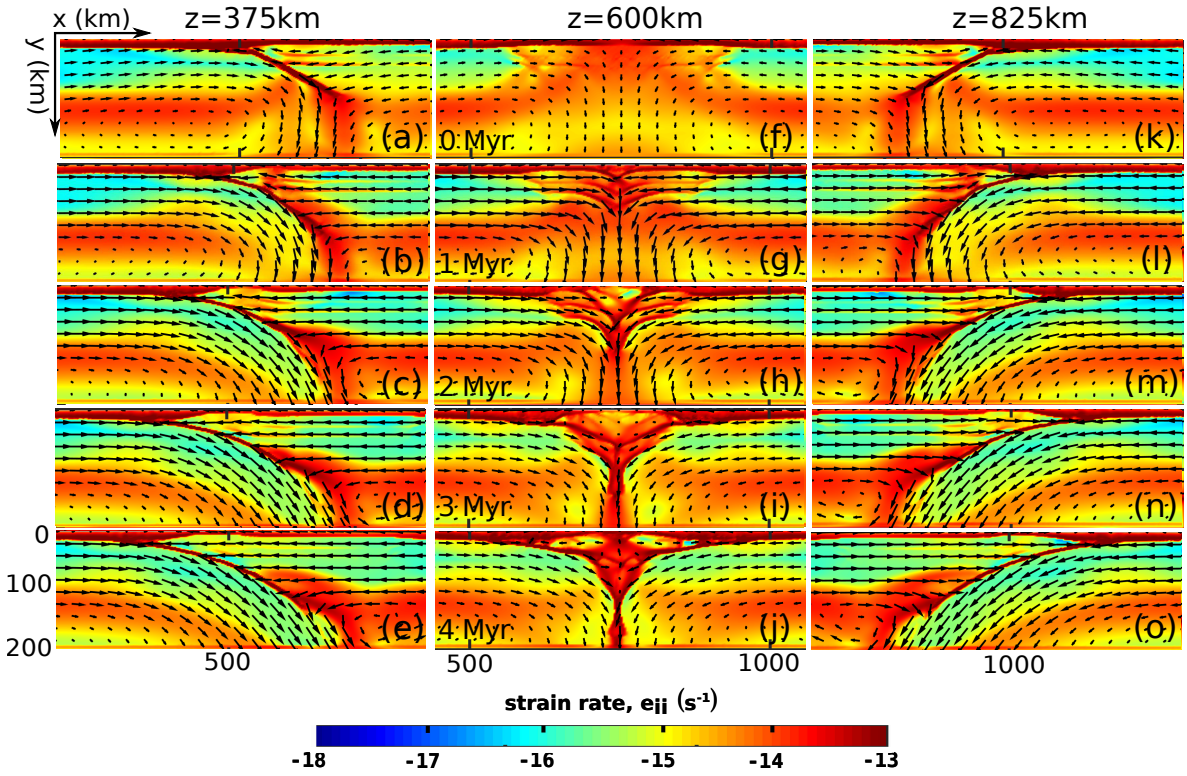

Figure B-6: Strain-rate of model *kitk*

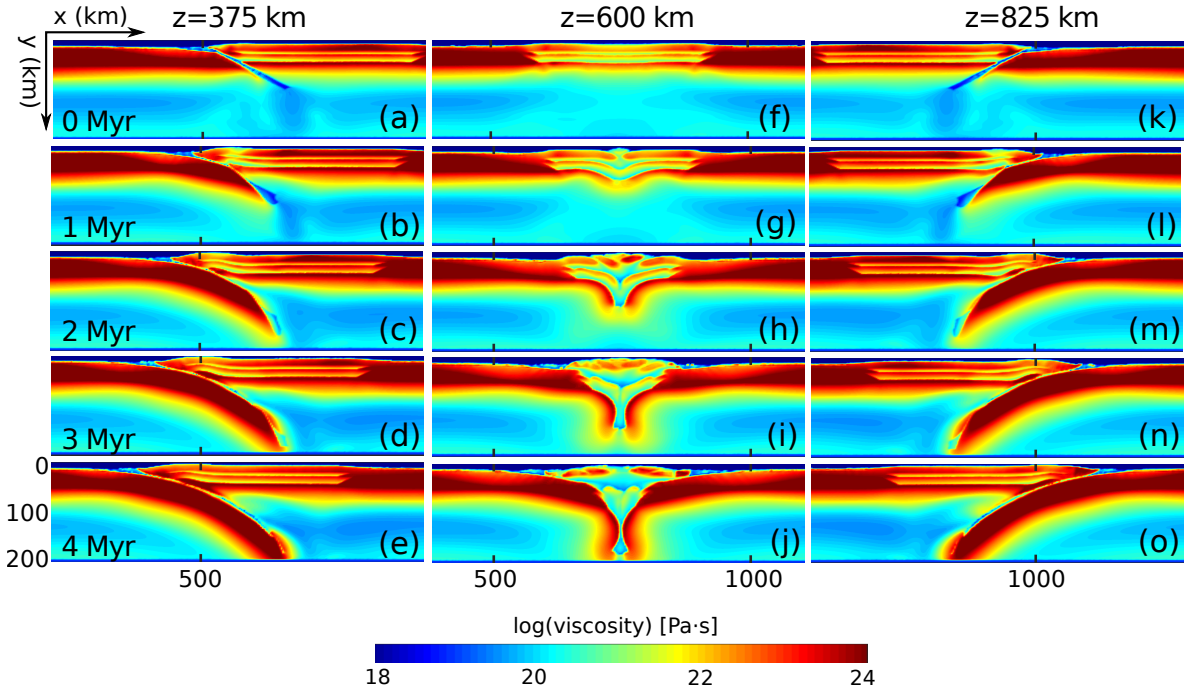

Figure B-7: Viscosity of model *kitk*

B-6 kitl visualisations

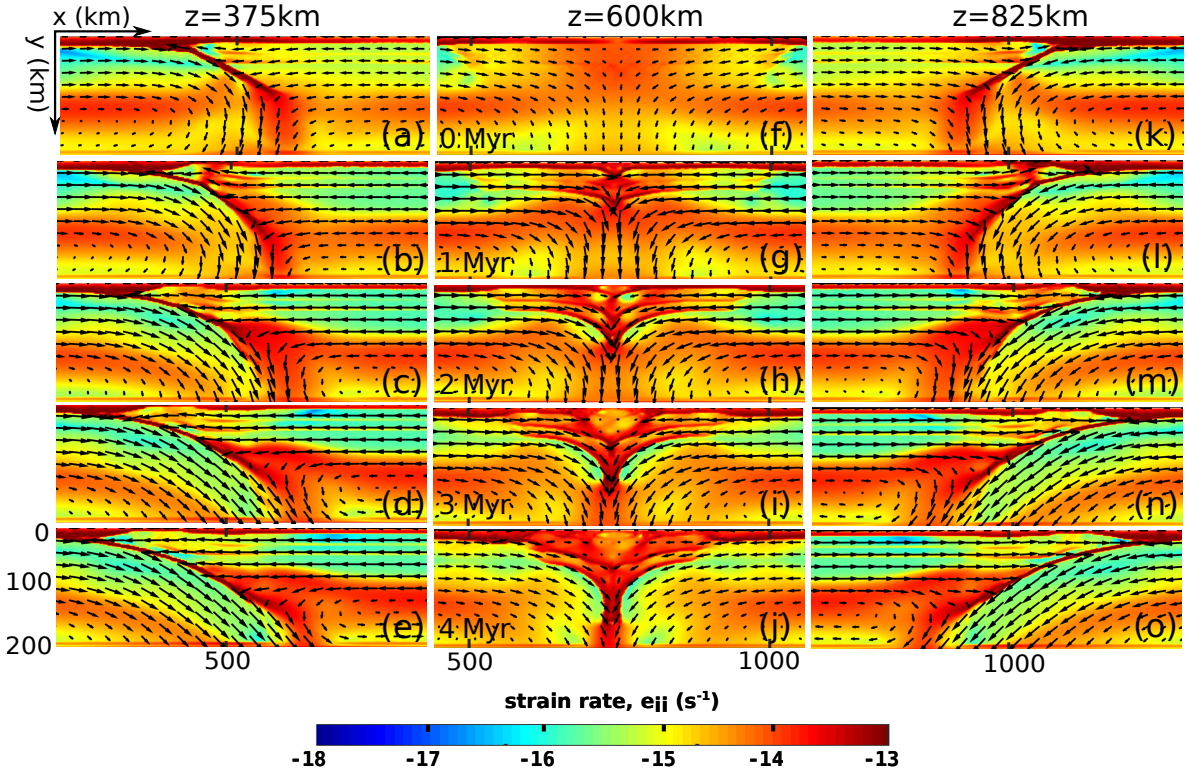

Figure B-8: Strain-rate of model *kitl*

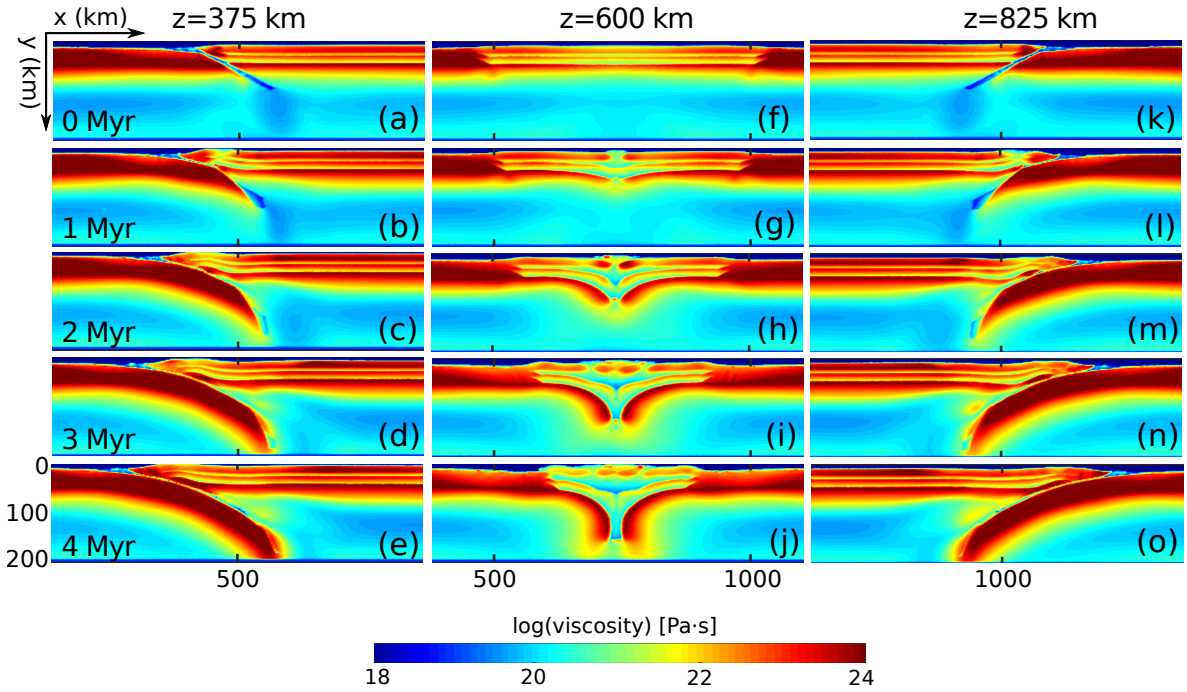

Figure B-9: Viscosity of model *kitl*